Urban Climate 56 (2024) 102041

Contents lists available at ScienceDirect

Urban Climate

journal homepage: www.elsevier.com/locate/uclim

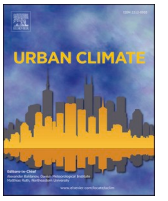

Data driven design for urban street shading: Validation and application of ladybug tools as a design tool for outdoor thermal comfort

Sinéad Nicholson [a,b,*], Marialena Nikolopoulou [a], Richard Watkins [a], Monika Löve [b], Carlo Ratti [b,c,d]

[a] Kent School of Architecture and Planning, University of Kent, Canterbury, CT2 7NR, UK
[b] CRA—Carlo Ratti Associati, Turin, Italy
[c] MIT, Cambridge, MA, USA
[d] Politecnico di Milano, Milano, Italy

ARTICLE INFO

Keywords:
Microclimate simulation
Mean radiant temperature
Lightweight shading
Ladybug tools
Urban design

ABSTRACT

Lightweight shading devices like sails, canopies, and street-scale shelters are a key strategy for urban cooling. Studies indicate that interactions between characteristics such as height, thermal emissivity and color, significantly affect outdoor thermal comfort, and those effects vary considerably with local context and time. However, practical understanding of shading often focuses solely on blocking direct solar radiation. Integrating microclimate simulation into design workflows can optimize shade design by considering all thermal effects. This paper validates two workflows using Ladybug Tools (LBT) for modelling freestanding shade, proposing their design applicability. A novel workflow models shortwave and longwave effects of lightweight shade materials on outdoor thermal comfort, differing from LBT's standard approach by considering shade interactions in longwave radiation exchanges. Simulated mean radiant temperature (MRT) is validated against field measurements and compared across both workflows. Field measurements separate long and shortwave contributions for accurate MRT comparison, revealing LBT's tendency to overestimate shortwave radiation effects. The custom workflow is applied to a design case study in Turin, Italy, evaluating various shade materials and their effects on MRT. Results demonstrate how shade material, height, ground material, and time of day interact to influence cooling effects, emphasizing practical implications for optimizing shade design.

1. Introduction

Urban populations across the middle to high latitudes are experiencing extreme periods of heat stress due to the intersecting pressures of global warming and the urban heat island effect. Without measures to maintain and improve the thermal comfort of urban outdoor spaces, the streets, squares, courtyards, and parks that constitute urban public space are at risk of becoming unusable. This impacts the health and well-being of urban inhabitants (Carleton et al., 2020), increases energy demands (Santamouris, 2021) and

* Corresponding author at: 30 Marana Ave, Rose Bay, Tasmania 7015, Australia.
E-mail addresses: skn26@kent.ac.uk (S. Nicholson), m.nikolopoulou@kent.ac.uk (M. Nikolopoulou), r.watkins@kent.ac.uk (R. Watkins), monika@carloratti.com (M. Löve).

https://doi.org/10.1016/j.uclim.2024.102041
Received 1 April 2024; Received in revised form 20 June 2024; Accepted 22 June 2024
Available online 6 July 2024

undermines urban civic life and community engagement (Francis et al., 2012), diminishing the overall resilience of cities to climate change.

1.1. Thermal comfort & urban shading

Thermal comfort can be measured through different indices, the most common being the Universal Thermal Comfort Index (UTCI), and the Physiological Equivalent Temperature (PET). They serve to translate meteorological and thermo-physical parameters including air temperature, wind speed, relative humidity, radiation fluxes, clothing level and metabolic rates into a predicted thermal experience (Höppe, 1999; Jendritzky et al., 2012).

Solar radiation has been shown to be the strongest indicator of potential thermal stress during warm conditions (Kántor and Unger, 2011). Shading is an effective urban cooling strategy, due primarily, to its ability to modify solar radiation in the streetscape (Emmanuel et al., 2007; Kántor and Unger, 2011; Nikolopoulou and Lykoudis, 2006; Thorsson et al., 2004). It does so through the interception of solar radiation, which is either reflected away, transmitted, or absorbed and emitted as heat. As this study is concerned with the influence of shading on thermal comfort, it focuses specifically on Mean Radiant Temperature (MRT), which describes the effect of the radiation fluxes on the human body and is a key input for the calculation of outdoor comfort indices such as PET and UTCI. In outdoor settings, MRT can range between −20 °C to +80 °C at the extremes (Weeding et al., 2024), and varies significantly across small spatial and temporal scales due to the diversity of elements in the urban streetscape, including topography, building geometries, surface material properties, street furniture, greenery and water features, in combination with changing sky conditions (Aviv et al., 2021; Merchant et al., 2022). This diversity requires targeted, street scale interventions to appropriately mitigate solar radiation and meet the specific thermal comfort needs of the space.

1.2. Urban street shading

Urban shading is generally categorized into building shade, tree shade and lightweight/artificial shade (Kántor et al., 2018; Lee et al., 2018; Middel et al., 2021; Watanabe et al., 2014). The latter two both provide options for targeted interventions at the street scale, compared to shading from buildings, which, although having the greatest cooling effect (Lee et al., 2018), is best suited to new urban developments.

Urban trees provide significant cooling primarily through dense, layered canopy shade and evapotranspiration (Armson et al., 2013; Colter et al., 2019a; Ettinger et al., 2024; Jareemit and Srivanit, 2022; Kántor et al., 2018; Meili et al., 2021; Zhang et al., 2023). However, as living systems, there are limitations in their implementation in urban areas. Horváthová found that the high costs of implementing and maintaining street trees can outweigh their cooling benefits for the first 20 to 30 years. Additionally, dense tree canopies can reduce air flow, increasing temperatures, nighttime heating, and local air pollution (Coutts et al., 2016; Meili et al., 2021), and have been associated with higher asthma and allergy rates (Sedghy et al., 2018). In comparing urban trees with lightweight structures, Middel et al. (2021) found only certain tree species with dense canopies, provided better cooling effects then lightweight shade structures, and Shashua-Bar et al. (2011) found a shade tree had marginally better cooling effects than a black mesh shade cloth, when both shared similar coverage and transmissivity. In both cases, the shading from the lightweight structures have the potential for improvement through design.

Lightweight shade devices, such as shade sails and street shelters, though lacking some of the social and environmental benefits of trees (Chiang et al., 2017; Meili et al., 2021), offer flexible shading with minimal infrastructure, maintenance, or space requirements. These devices are easy to implement in a range of urban spaces, enabling ‘thermal retrofitting’ (Cortesão et al., 2013), especially in compact spaces, where trees cannot grow. They provide low-cost cooling, addressing urgent shade needs and urban inequality (Harlan et al., 2007), and can adapt to changing thermal conditions through easy installation, retraction, or removal. They also offer opportunities for highly optimized shading, balancing shade requirements with other requirements such as visibility or ventilation. Finally, lightweight shading offers opportunities to integrate multifunctional and innovative materials, such as photovoltaic canopies (Middel et al., 2016), retroreflective shading for urban canyons (Castellani, 2021), or temporary shelters with radiative cooling properties able to provide cool ‘oases’ among hot streets (Calabrò et al., 2015).

Research on the impact of lightweight shading on outdoor thermal comfort focuses primarily on its capacity to block direct solar radiation. Multiple studies have highlighted the cooling effects associated with this characteristic of lightweight shade, while also identifying significant effects arising from other shade properties that remain less explored, as well as the complexity of predicting the result of the combined effects across different contexts (Colter et al., 2019a; Elgheznawy and Eltarabily, 2021; Kántor et al., 2018; Lee et al., 2018; Middel et al., 2016, 2021). For instance, Colter et al. (2019b) found that while lightweight structures effectively reduced solar radiation, they didn’t correspondingly enhance perceived thermal comfort compared to shade from trees, associating the difference to unstudied effects of the shade material. Work by Middel et al. (2021), Merchant et al. (2022), Shashua-Bar et al. (2011) and Tang and Li (2022), emphasized the potential contributions of longwave radiation due to shade material properties, and the varying differences due to changes in the surrounding streetscape. Studies that have investigated specific shade properties such as material emissivity and reflectivity, color or height, reveal notable differences in cooling effects. Rossi et al. (2020, 2022), identified significant reductions in MRT with low emissivity materials. Garcia-Nevado et al., 2020) highlighted the non-linear relationship between increasing shade material openness factor and increasing pavement temperatures, while Kántor et al. (2018) observed variations in cooling effects based on shade sail height. These findings provide a more nuanced understanding of the effects of various properties of lightweight shading, but they also illustrate the complex interplay between shade properties and the local surroundings. This complexity requires further research to understand the multifaceted effects of lightweight shading.

1.3. Microclimate simulation for shade design: ladybug tools

A design approach utilizing microclimate simulation can support designers (and researchers) in navigating the complexity of outdoor thermal comfort and optimizing urban shading. The most commonly used software in the literature on outdoor thermal comfort is ENVI-met (McRae et al., 2020; Toparlar et al., 2017). Others such as RayMan (Matzarakis et al., 2010), Solweig (Lindberg et al., 2008) and CitySimPro (Robinson et al., 2009) are available but ENVI-met (Bruse, 2004), is considered the most comprehensive for a wide range of microclimate studies, due to its incorporation of computational fluid dynamics (CFD) in the modelling processes. However, it is standalone software, with limited 3D modelling capabilities and long simulation times due to the CFD. This limits its use as a design tool, where rapid feedback in the early design stages is essential (Erell et al., 2011). The software best matched to design requirements does not separate the design and analysis process - a major constraint identified by architects when interviewed over integrating environmental design into practice (Weytjens et al., 2011). Ladybug Tools (LBT) (Mackey and Roudsari, 2023) is a free and open-source parametric plug-in providing environmental analysis capabilities including microclimate simulation within computer aided design (CAD) software such as Rhinoceros (McNeel and Others, 2010). As a parametric plug in, it allows users to customize workflows for specific design problems and assess the effects of multiple parameters such as geometries, material properties; climates and urban form, in a rapid and iterative manner, within a familiar design platform and at a scale not possible in empirical/physical studies. This is essential in developing strong feedback in the design process and connecting data with design.

LBT's use in simulating outdoor thermal comfort for street canyons, courtyards or public spaces has been validated in several studies (Elrefai and Nikolopoulou, 2023; Elwy et al., 2018; Evola et al., 2020; Ibrahim et al., 2020; López-Cabeza et al., 2022; Sun et al., 2023), with its accuracy in simulating MRT found to be comparable with EnviMET (Ibrahim et al., 2020). However, Elwy et al. (2018), Evola et al. (2020) and Elrefai and Nikolopoulou (2023) found a tendency to overestimate MRT in direct sunlight. All the studies except Elrefai and Nikolopoulou (2023) use a legacy version of LBT, which has been superseded by LBT plus, and included improvements to its MRT calculations. The focus of these studies is at neighborhood scales which does not allow in-depth analysis of lightweight shading (referred to as free-standing shade in simulation literature). At the smaller scales, literature on LBT is focused on its use in designing street shading rather than validation (Alharthi and Sharples, 2020; Chi et al., 2021; Lucarelli and Carlo, 2020; Mackey et al., 2015; Rodonò et al., 2020) and the limitation of the tool in only considering free-standing shade in shortwave calculations is highlighted (Rodonò et al., 2020). Vartholomaios and Kalogirou (2020) demonstrates the application of LBT in the design process, taking advantage of its parametric characteristics to develop a workflow that provides matrices highlighting the difference in cooling effect with changes to height and protrusion characteristics.

1.4. Study aims

The literature suggests there is an opportunity to improve outdoor thermal comfort through a more comprehensive understanding of the performance of lightweight shading. It also highlights the difficulty of predicting the performance of lightweight shading due to the interactions between shade material, form and temporal and spatial context and their impact on MRT. Since implementation of street shading lies primarily with architects and designers (Santos Nouri et al., 2018) methods for understanding their complex effects on thermal comfort should be embedded into the design process. LBT provides a tool to navigate this complexity in designing shade due to its accessibility as a design tool and its parametric capabilities. However, validation of MRT simulations from the updated LBT is required. Additionally, LBT only considers lightweight (free-standing) shade in *shortwave* calculations for MRT, thus limiting analysis of shading effects and opportunities for design optimization.

This paper, therefore, aims to evaluate the use of LBT as a tool to support data-driven design of lightweight shading devices. It evaluates LBT's predictions of MRT under shade and presents a customized workflow for modelling both shortwave and longwave effects of free-standing shade. In the first section LBT's performance in simulating MRT below a freestanding shade textile is compared to field measurements. A 'standard' workflow using default LBT components, which considers the effect of the shade only in shortwave calculations, is compared against a 'SolAir' workflow which adds custom Python components to the standard workflow so that the shade's longwave contribution to MRT is included. The use of a novel sensor capturing shortwave and longwave radiation in six directions, allows for separate validation of predicted surface temperatures, longwave mean radiant temperatures and shortwave mean radiant temperatures.

In the second section of the paper, the SolAir workflow is applied in the design of a shade canopy for an urban park in Turin, Italy. Parametric studies are conducted to investigate the effects of various combinations of shade materials, shade heights and ground materials. Four shade materials; glassfibre, thin film photovoltaic (PV), a white PVC coated polyester (PolyPVC) and an optimized high reflectivity/low emissivity foil (HighR/LowE) are tested at 2.4 m, 3 m and 5 m, with two different ground materials. The results show the significant resulting differences between the different parameter combinations on MRT, highlighting the importance of a data-driven approach to shade design, as well as material choices for outdoor thermal comfort.

2. Materials & methods

The methodology consisted of two parts: field work to collect MRT measurements below a shade textile, which provided data for use in calibrating and validating the LBT model; and microclimate modelling of free-standing shade using LBT. The former is described in Sections 2.1 to 2.5 and the latter in Sections 2.6 and 2.7.

2.1. Thermal metrics

MRT was the primary variable used for validation due to its significance for thermal comfort and its relevance in understanding shade performance, as discussed in Section 1.1. It considers longwave radiation exchanged between a person and surrounding surfaces and sky, as well as incident shortwave radiation on the person (Kántor and Unger, 2011), making it well adapted for outdoor comfort studies. Field measurements of MRT are predominately conducted through globe thermometers due to the lower cost and simpler set up (Johansson et al., 2014). However, a globe thermometer does not capture the spatial variation of MRT or distinguish between shortwave and longwave contributions, and has limitations related to lag times and accuracies dependent on precise air flow measurements (Aviv et al., 2021; Tang and Li, 2022).

This study uses an adapted version of the integral method (explained in Section 2.4), where short and longwave radiation using pairs of pyranometers and pyrgeometer are mounted horizontally and vertically, so as to capture incoming radiation in six directions (north, south, east, west and up and down) (Kántor and Unger, 2011). This is important for the purposes of this study for two reasons; to capture the spatial variation of MRT due to differences in surface temperatures, and to separate the LW and SW contributions to provide more in-depth metrics for validation of LBT. It also accounts for the different shortwave and longwave absorption coefficients exhibited by the human body and uses weighting factors based on a cylinder, providing a more accurate representation of the human body compared to the spherical globe sensor.

The radiation measurements can be converted to a total MRT value using Höppe's equation (Eq. (1)) which weights directional shortwave and longwave radiation with factors representing the amount of body exposed to the corresponding direction, and absorption coefficients representing the radiation absorbed and emitted by the human body. For a standing person, weighting factors of 0.06 and 0.22 are used for the longitudinal and lateral measurements, respectively. The shortwave absorption coefficient is dependent on characteristics such as clothing and skin color but typically set as 0.7 (Kántor and Unger, 2011). The longwave absorption coefficient for a human body is defined as 0.97 in Höppe, 1992, and is equivalent to the emission of a clothed human body following Kirchoff's law.

$$MRT = \sqrt[4]{\frac{\sum_{i=1}^{6} W_i(\alpha_k K_i + a_l L_i)}{\alpha_l \sigma}} - 273.15 \quad (1)$$

Where K_i is incident shortwave radiation (W/m^2), L_i is longwave radiation (W/m^2), σ is the Stefan-Boltzmann constant (W/m^2 K^4), W_i is the weighting factor, a_k is the shortwave absorption coefficient and a_l is the longwave absorption coefficient (all unitless).

2.2. Study site

The study site was selected based on two main conditions:

- Open and unshaded to simplify the model and isolate the effect of the shade device.
- The presence of a nearby meteorological station to provide precise data for model boundary conditions and calibration.

The selected site was the rooftop of the Polytechnic of Turin's Energy department and measurements were collected on 1st July 2023. The site is located in the Crocetta neighborhood of Turin, northern Italy (45°06′N, 7°66′E), as shown in Fig. 1, and is open and unshaded, with a ground consisting of exposed aggregate composite cement tiles. Turin experiences a warm temperate climate (Köppen climate classification Cfa) (Kottek et al., 2006), with typical minimum and maximum summer daytime temperatures ranging between 14 °C to 28 °C (CustomWeather, 2021). During the summer of the period of study, Turin was experiencing higher than average temperatures, reaching a daytime maximum of 34 °C and mean of 28.6 °C (San Maurizio Canavese, 2023, *Italy Weather History | Weather Underground*).

2.3. Site conditions

Metrological measurements of air temperature, relative humidity, wind speed and direction, global radiation, diffuse radiation, direct normal radiation and direct horizontal radiation were collected, for July 1st 2023, by the meteorological station on site, which was mounted approximately 1.8 m above the ground. During the period of study, the site experienced a minimum air temperature of 18.5 °C at 10:00 and maximum air temperature of 27.3 °C at 17:00. Wind speeds ranged between 1.7 and 2.2 m/s and relative humidity between 40% and 70% (Fig. 2).

2.4. Field measurements

MRT was measured using the high.RES sensor (Fig. 3) which is an adaptation of the integral method for measuring MRT, developed by CHAOSense Labs[1] and validated and described in more detail elsewhere (Aviv et al., 2021; Meggers et al., 2022; Merchant et al., 2022). The high.RES sensor takes radiation measurements in the north, south, east, west, and up and down directions. With each

[1] highRES sensor at *Research-Grade Radiant Sensors | Chaosense*

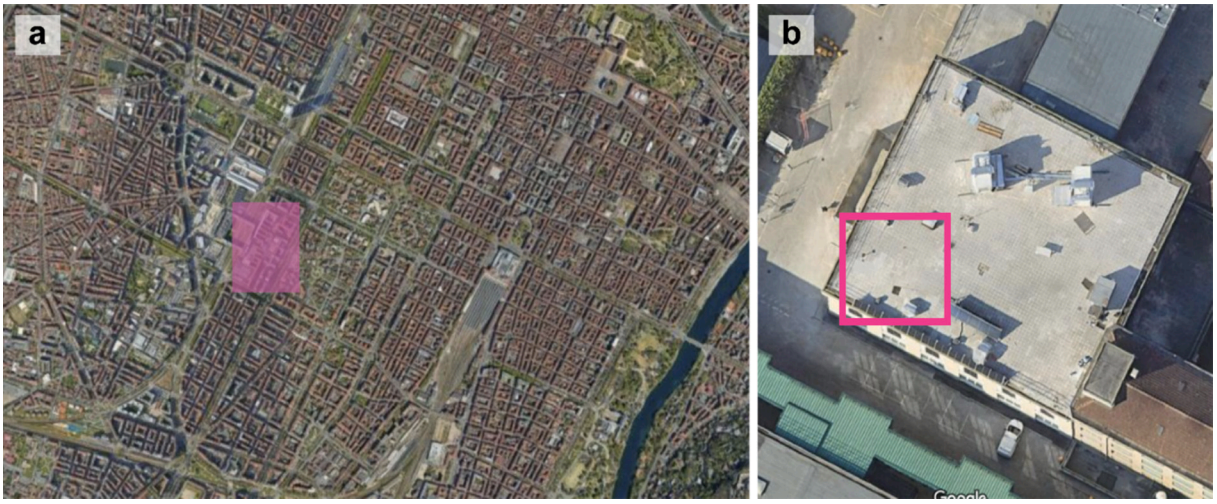

Fig. 1. **a**) Birds eye view of Turin highlighting the location of the Politecnico di Torino within the city **b**) close-up of the roof of the DENERG department where the field study was conducted.

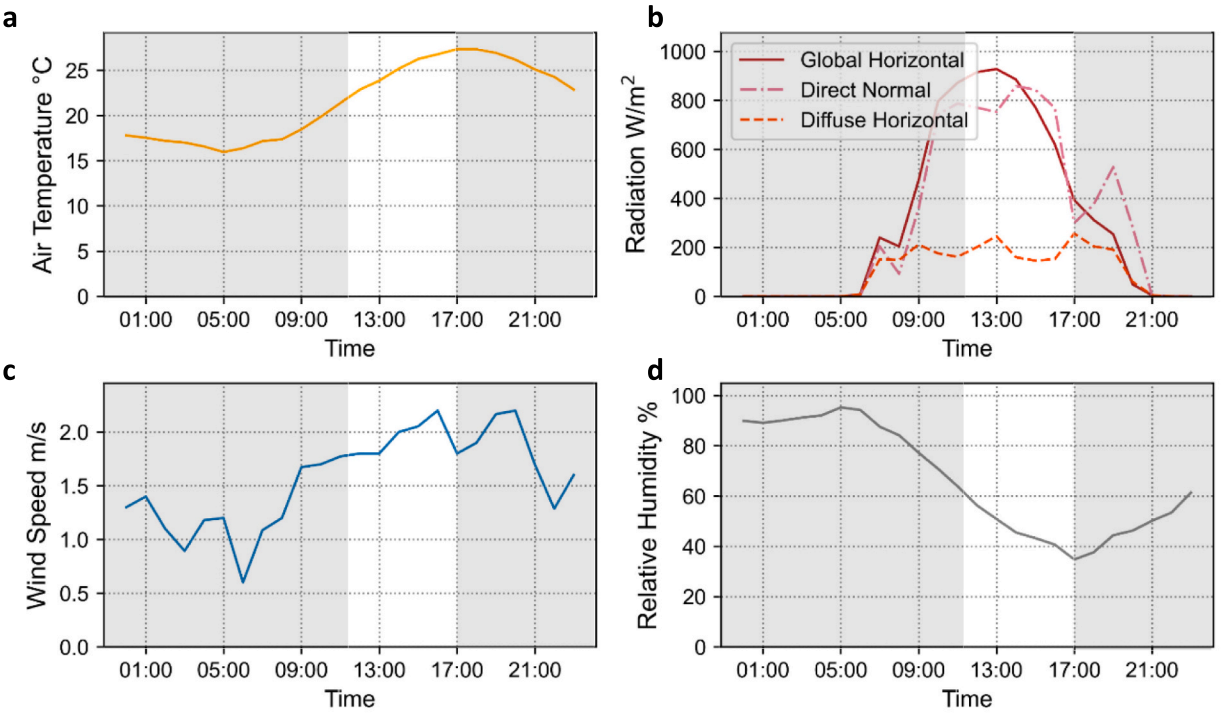

Fig. 2. Meteorological data at field study site on the Politecnico di Torino's roof, Turin, Italy on 1st July; ***a)*** Air temperature (°C), ***b)*** Global Horizontal radiation, direct normal radiation and diffuse horizontal radiation (W/m^2), ***c)*** Wind Speed (m/s), and ***d)*** relative humidity (%), provided by Politecnico Di Torino meteorological station, at 1.8 m above roof level. The actual period of MRT measurements is shown in white. The full 24 h were used for model calibration.

direction, shortwave and longwave radiation data are collected allowing for a thorough analysis of how HB performs in simulating MRT, since surface temperatures, SW MRT and LW MRT can be compared in addition to the total MRT. Specifications of the sensors used to measure meteorological conditions, and the radiation below the shade are listed in Table 1.

The shade textile was positioned 0.8 m above the ground as shown in Fig. 4 and aligned so that one edge was parallel to due south. A 1x1m sample of a glassfibre textile was used, with material properties including measured emissivity and reflectivity values, provided by the manufacturer (see Table 2). This allowed for precise calibration of the microclimate model. The exact ground properties were

Fig. 3. The high.RES sensor for measuring Mean Radiant Temperature from CHAOSense Labs.

unknown, therefore, are assumed based on the EnergyPlus (E+) Database of material thermal properties.

The high.RES sensor was positioned below the shade textile and in the center of the shade area. It was mounted on a tripod 60 cm from the ground to ensure the textile filled the entire field of view of the upwards sensor. Short and longwave radiation was collected from 9:00 to 17:00 at one-minute intervals.

2.5. Data analyses

The surface temperatures used for model calibration, and the SW MRT, LW MRT and final MRT were calculated from the radiation measurements of the high.RES sensor. All measurements were averaged to 5 min intervals and several steps were then taken to process the data and prepare it for use in Höppe's integral equation (Höppe, 1992) (Eq. (1)) to calculate the MRT value. The individual steps are described in the following paragraphs.

2.5.1. Surface temperatures

The radiant temperatures measured by the up and down sensors were converted to surface temperatures using the Stefan Boltzmann Law: $P/A = \epsilon\ \sigma\ T^4$ [W/m^2] where P is radiant power *(W)*, A is surface area in m^2, ϵ is thermal emissivity, σ is the Stephan Boltzmann constant [W/m^2 K^4], and T is the radiant temperature (K). The high.RES infrared sensors take readings with an assumed emissivity of 1, therefore, radiant energy *(P)* was first calculated with an emissivity of 1, and surface temperatures were calculated from the resulting radiant energy using an emissivity of 0.78.

2.5.2. LW MRT

The radiant temperatures from all six directions were converted from Celsius to W/m^2 using Boltzmann's Law. LW MRT values were then calculated using Eq. (1) (Section 2.1) by excluding the shortwave component ($\alpha_k K$). The longwave absorption coefficient was changed from 0.97 to 0.95 to match that of LBT's default.

2.5.3. MRT

Total MRT values were calculated using Eq. (1) and including the shortwave component (α_kK). The shortwave absorption value (α_k) of 0.70 represents medium level of clothing and light skin and is the default in LBT. Weighting factors are the same for shortwave and longwave components.

2.5.4. SW MRT

The LW MRT was subtracted from the total MRT to calculate the SW MRT, also described as the SW delta in LBT.

All resulting data sets (surface temperatures LW MRT, SW MRT and MRT) were averaged to hourly intervals for comparison with HB's outputs since HB is currently limited to hourly timesteps for UTCI analysis.

2.6. Modelling

LBT functions as an interface, connecting a CAD model and a range of material, geometry and environmental parameters to the

Table 1
Sensor Specifications.

Parameter Measured	*Sensor*	*Accuracy*	*Range*	*Response Time*
Radiant Temperature (°C)	MLX90614 IR, 90° FOV (high.RES cube)	±0.3 °C	0 to 50 °C	
Shortwave Radiation (W/m^2)	Custom (high.RES cube)	Estimated 5–7%	0.2-2 μm	
Air Temperature (°C)	Thermocouple Type B (Model unknown[1])	±0.25 °C	−40 to 85 °C	<1.0 s
Global Horizontal & Diffuse Radiation (W/m^2)	Delta-T SPN1 Sunshine Pyranometer	±5% ±10 W/m^2 Hourly averages	0 to >2000 W/m^2	0.1 s
Wind Speed & Direction (m/s)	Cup & Vane Anemometer (Model unknown[2])	±0.3 m/s ≤ ± 3°	0-45 m/s 0–360°	3.0 s

[1] Thermocouple Ambient Air Temperature Measurement PPL10-T. (n.d.). *Process Parameters Ltd.* Retrieved Feb 3, 2024, from https://www.processparameters.co.uk/thermocouple-sensors/thermocouple-for-ambient-air-temperature-measurement-ppl10-t/

[2] *Rk120-01c Combined Wind Speed & Direction Sensor | Rika Sensors*. (n.d.). Retrieved March 31, 2024, from https://www.rikasensor.com/rk120-01c-combined-wind-speed-direction-sensor-1.html

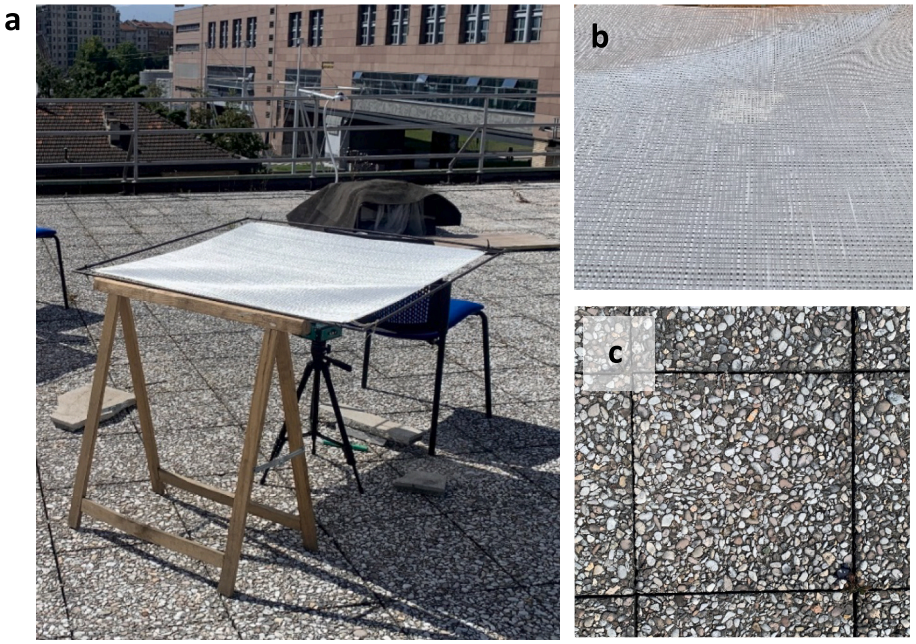

Fig. 4. a) Experimental set up of the study showing the high.RES sensor mounted beneath the 1m^2 glassfibre textile **b)** close up of the glassfibre textile **c)** close up of the aggregate cement tile.

necessary simulation engines: EnergyPlus (U.S. Department of Energy, 2022a, b) and Radiance (Greg Ward, 2021) for energy, radiation and daylighting studies and OpenFOAM (OpenCFD Ltd, 2022) for fluid processing. The version used in the work presented here is version 1.7. To simulate MRT, users of LBT can either perform simplified calculations through the data analysis and visualization subsection of components in LBT, called Ladybug, or more comprehensive simulations through LBT's subsection of energy modelling and daylight simulation components, called Honeybee (HB). HB allows energy modelling and sophisticated ray tracing through the open-source simulation engines EnergyPlus (E+) and Radiance and is the chosen approach in this paper since it allows calculations of surface temperatures and more accurate ray tracing for calculating view factors and radiation paths.

The specific component used in simulating MRT through HB is the 'UTCI Comfort Map' (UTCI Map), which outputs an air temperature, and calculated LW MRT, SW MRT and total MRT, alongside the final universal thermal comfort index (UTCI) values.[2] The MRT equations are derived from ASHRAE 55's SolarCal method (see Arens et al., 2015) and the E+ Engineering Reference (U.S. Department of Energy, 2022a, b). The adaptation of the equation for LBT is given in Appendix A.1.

The simulation process involved four steps: setting boundary conditions, geometry modelling, conversion to HB zone, and running the simulation. We tested two workflows for setting up the simulations: the Standard workflow, where shade surfaces are modelled as 'context' and discounted from energy calculations, and the SolAir workflow, which is an extension of the Standard workflow, and uses customized components to include the shade surface in energy calculations. The workflows were adapted from two example scripts

[2] Find source code at (https://github.com/ladybug-tools/ladybug-comfort/blob/master/ladybug_comfort/map/mrt.py#L176)

Table 2
Material properties of Glassfibre textile from manufacturer data sheets.

Material Properties	Glassfibre
Thickness (m)	0.003
Conductivity (W/m-K)	2.05[1]
Density (Kg/m^3)	2600[1]
Specific Heat Capacity (J/kg-K)	593[1]
Roughness	Smooth
Emissivity	0.78[2]
Reflectivity	0.71[2]
Openness Factor	0.1

[1] *i-Mesh | Technical Properties: Sustainable, Strong, Light, Durable Fabric*. (n.d.). Retrieved July 2, 2024, from https://www.i-mesh.eu/technical

[2] Cardinali, M., Gambelli, A. M., Piselli, C., Filipponi, M., Castellani, B., Nicolini, A., & Rossi, F. (2019). *Experimental analysis and optimization of outdoor curtain materials for solar protection as a solution for urban heat island mitigation and thermal comfort improvement*. 12.

used to simulate MRT in a street canyon, and surface temperatures underneath a tree canopy (Chris Mackey, 2016a, 2016b). The individual steps for both workflows are illustrated in the schematic in Fig. 5.

In the Standard workflow, modelling shade as context assumes that shade surfaces follow air temperature and are not considered in longwave calculations but allows a reflectance value and transmittance schedule which can approximate the openness factor of the shade material. In the SolAir workflow, shortwave calculations remain the same but consideration of the longwave contribution by the shade to MRT is included. This allows more customization of the material properties and a surface temperature to be calculated for inclusion in LW MRT. The four common stages of the workflows are described in the following paragraphs, and the additional steps of the SolAir workflow described in Section 2.5.2.

2.6.1. Setting up the model

2.6.1.1. Boundary conditions. Honeybee relies on an E+ weather file (EPW) to set the boundary conditions. An EPW database can be accessed through the LB EPW map component, where the appropriate EPW is downloaded. Out of the four available EPW's for Turin, ASHRAE's 2021 Typical Meteorological year (TMYx) EPW was chosen, being the most recently updated and closest in proximity to Turin. Air temperature, wind speed, relative humidity, and direct and diffuse radiation data from the Polito weather station were averaged to hourly intervals and inserted into the list of corresponding data sets of the weather file, replacing the original EPW values for the analysis day. The availability of on-site meteorological data allowed precise calibration of the boundary conditions for the simulations reducing the number of variables that could explain the differences between measured and simulated values.

2.6.1.2. Geometry. The shade textile and chair supporting the textile were modelled as planar surfaces. The ground was modelled as a $6 \times 6 \times 0.2$ m box, splitting the top surface of the ground geometry into grid faces of 0.25m^2. The resolution of the ground grid was chosen after a series of tests, comparing the measured ground temperature with an average of selected HB ground face temperatures, and found 0.25m^2 to correspond best with measured values. The shade textile was modelled as a single planar surface of 0.9×0.9 m. The final geometry is shown in Fig. 6.

2.6.1.3. Honeybee zone. The ground was converted into an HB Room and ground properties were applied using HB 'Make Ground' Component. The chair supporting the shade, and the shade surface were converted into shade objects through the 'HB Shade as Context' Component. Ground material properties were taken from a default E+ stone material with adjusted reflectivity and are shown in Table 3. To translate the properties of the glassfibre textile to an HB shade the measured reflectivity of 0.71 was used and a transmissivity of 0.1 was given to represent the textile's openness factor of 10%. For the SolAir workflow, emissivity was assumed to equal thermal absorption, a roughness factor of Smooth was selected based on E+ recommendations (U.S. Department of Energy, 2022a, b, Section 3.5.5.1, pg. 96) and a solar absorption value was calculated by subtracting transmissivity and reflectivity from 1. Properties are shown in Table 3.

2.6.1.4. Simulation. HB objects were combined into an HB model with a sensor point added to represent the position of the field sensor. Body characteristics and Radiance parameters were left to defaults and analysis period set for 1st July. Different Radiance parameters,[3] relating to how indirect and reflected radiation were treated in the simulation, were trialed until the resulting SW MRT

[3] https://floyd.lbl.gov/radiance/refer/Notes/rpict_options.html.

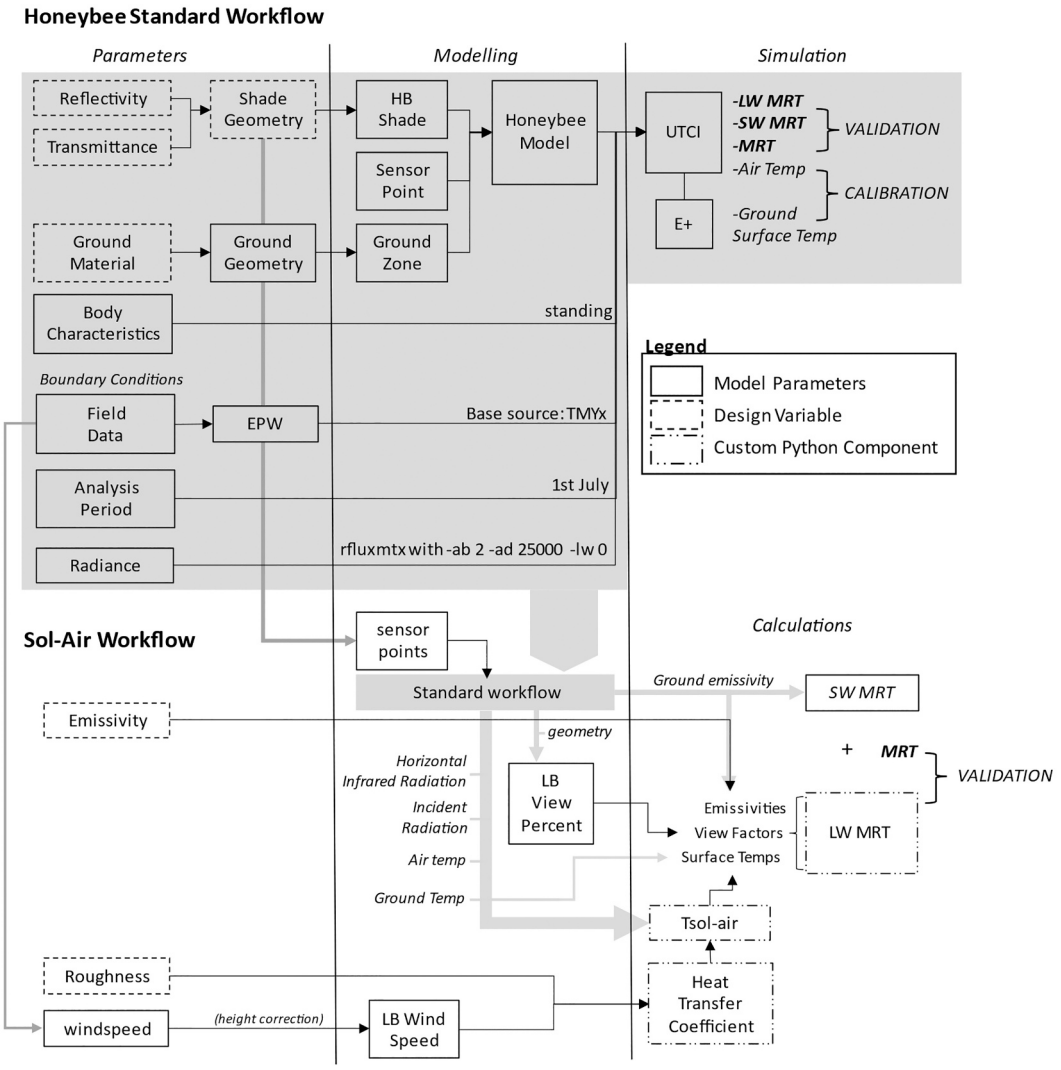

Fig. 5. Schematic illustrating the Standard and SolAir workflows used to simulate MRT with Ladybug Tools. The Standard workflow is highlighted in gray, and the SolAir workflow is shown as an extension of the Standard workflow. Custom components are outlined in dash/dot boxes and design variables are outlined in dotted boxes. All inputs in the parameters section are variables that can be altered individually for iterative studies on MRT. The data output by the workflows is identified at the right of the schematic and labeled if used as validation or calibration metrics.

values remained relatively stable with each simulation run. Highest accuracy settings were used but ambient bounces were limited to two as with a larger number the predicted SW MRT was unrealistically high. This ensures the sensor 'sees' radiation reflecting off the ground and underside of the shade surface but impacts on the stability of the SW MRT calculation. This is discussed further in the results section. Results for MRT, LW and SW MRT and air temperature were extracted from the UTCI component and surface temperatures were extracted from the SQL file created by the E+ section of the simulation. Air temperature and ground temperature were used for model calibration, with air temperature taken at the sensor point and ground temperature taken as an average of the faces directly underneath the shade as shown in Fig. 3 in purple. The grid squares selected for averaging were those that filled the field of view in the downwards pointing sensor of the high.RES sensor.

2.6.2. SolAir workflow – a customized approach

In the SolAir workflow, additional steps were added to the Standard workflow to calculate the shade surface temperature, and to include it, and surface emissivities in the LW MRT calculation. The SolAir eq. (O'Callaghan and Probert, 1977) (Eq. (2)) defines the effective outdoor air temperature that would produce the equivalent temperature distribution and heat transfer through a surface as the combination of incident radiation, convection and radiation transfer to sky and surrounding surfaces (see Appendix A.2 for Equations). It can be used to predict the surface temperature of an exposed external surface, factoring in absorbed radiation and convective heat exchange with the surrounding air based on material properties. It does not consider temperature changes through

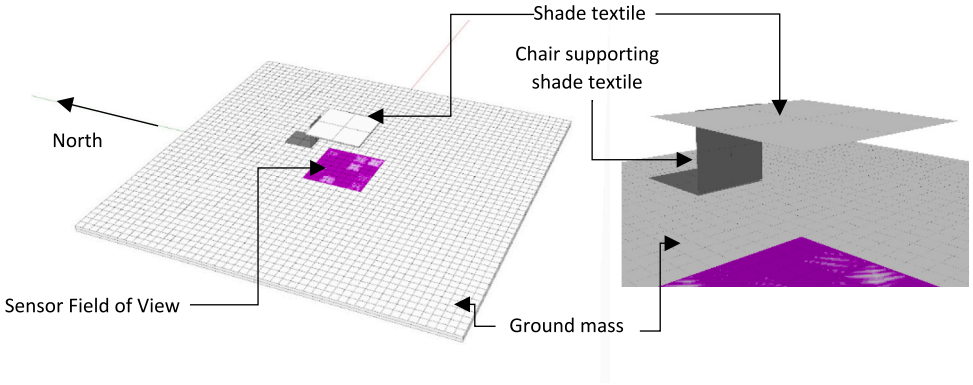

Fig. 6. Honeybee CAD model showing ground grid, textile and chair shade surfaces. The purple squares indicate the faces used for ground surface temperature extraction representing the field of view of the infrared sensor. (For interpretation of the references to color in this figure legend, the reader is referred to the web version of this article.)

Table 3
Material properties of Glassfibre textile and Cement aggregate tile, presented as they were input in the Honeybee model with the Glassfibre openess factor converted to transmissivity. Those marked with an adj signify the values were adjusted during the calibration process.

Material Properties	*Aggregate Cement Tile*	Material Properties	*Glassfibre*
Thickness (m)	0.2		
Conductivity (W/m-K)	3.00		
Density (Kg/m^3)	2700		
Specific Heat Capacity (J/kg-K)	790	Transmissivity	0.1
Roughness	Rough^{adj}	Roughness	Smooth
Thermal Absorptance	0.96	Emissivity	0.78
Solar Absorptance	0.65^{adj}	Reflectivity	0.71

conduction or heat storage. Details of its use in modelling the impact of high-albedo materials on outdoor thermal comfort can be found in Erell et al. (2014).

$$T_{sol-air} = T_o + \frac{a \bullet I - \Delta Q_{ir}}{h_o} \quad (2)$$

Where T_o is Ambient temperature *(K),* $I$is Global solar irradiance *(W/m^2),* a is surface solar absorptance which is unitless, $\Delta Q_{ir}$is net longwave radiation at the surface *(W/m^2)* and $h_o$is the combined heat transfer coefficient *(W/m^2K).*

The equation was split into simulation of incident radiation on the shade's surface, calculation of the heat transfer coefficient, calculation of the resulting SolAir Temperature, and calculation of the resulting LW MRT. The latter three steps rely on custom Python components, the code for which are provided in Appendix B.1,B.2 and B.3. The steps are described more detail in the following paragraphs.

2.6.2.1. Step 1 Incident radiation (I). Additional sensor grids above and below the shade were added to the model and the incident radiation captured by the sensors was extracted from the UTCI component.

2.6.2.2. Step 2 Combined heat transfer coefficient (h_o). Custom Python functions were used to calculate the heat transfer coefficient using the SIMPLECombined Method as described in the E+ Engineering Reference (U.S. Department of Energy, 2022a, b Section 3.5.5, pg. 95). Wind speeds were taken from the EPW and adjusted for sensor height using the LB Wind Speed Component. The shade material roughness determined the coefficients used in the calculation of the heat transfer coefficient.

2.6.2.3. Step 3 SolAir temperature. The incident radiation determined in step 1 was multiplied by the shade absorptivity minus transmissivity.

The net longwave radiation (ΔQ_{ir}) was split into exchange between the shade and sky, and exchange between the shade and ground. The radiation exchanges were calculated using equations taken from the outside surface heat balance section of the E+ Engineering reference (U.S. Department of Energy, 2022a, b, Section 3.5.2, pg. 90). For these equations ground temperature and air temperature from the Standard workflow were used, with the air temperature as the starting shade temperature. Horizontal infrared radiation was taken from the EPW file to calculate sky temperature. Form factors were assumed to be one for a horizontal surface in an open area. The resulting longwave radiation flux was subtracted from the shortwave contribution and divided by the heat transfer

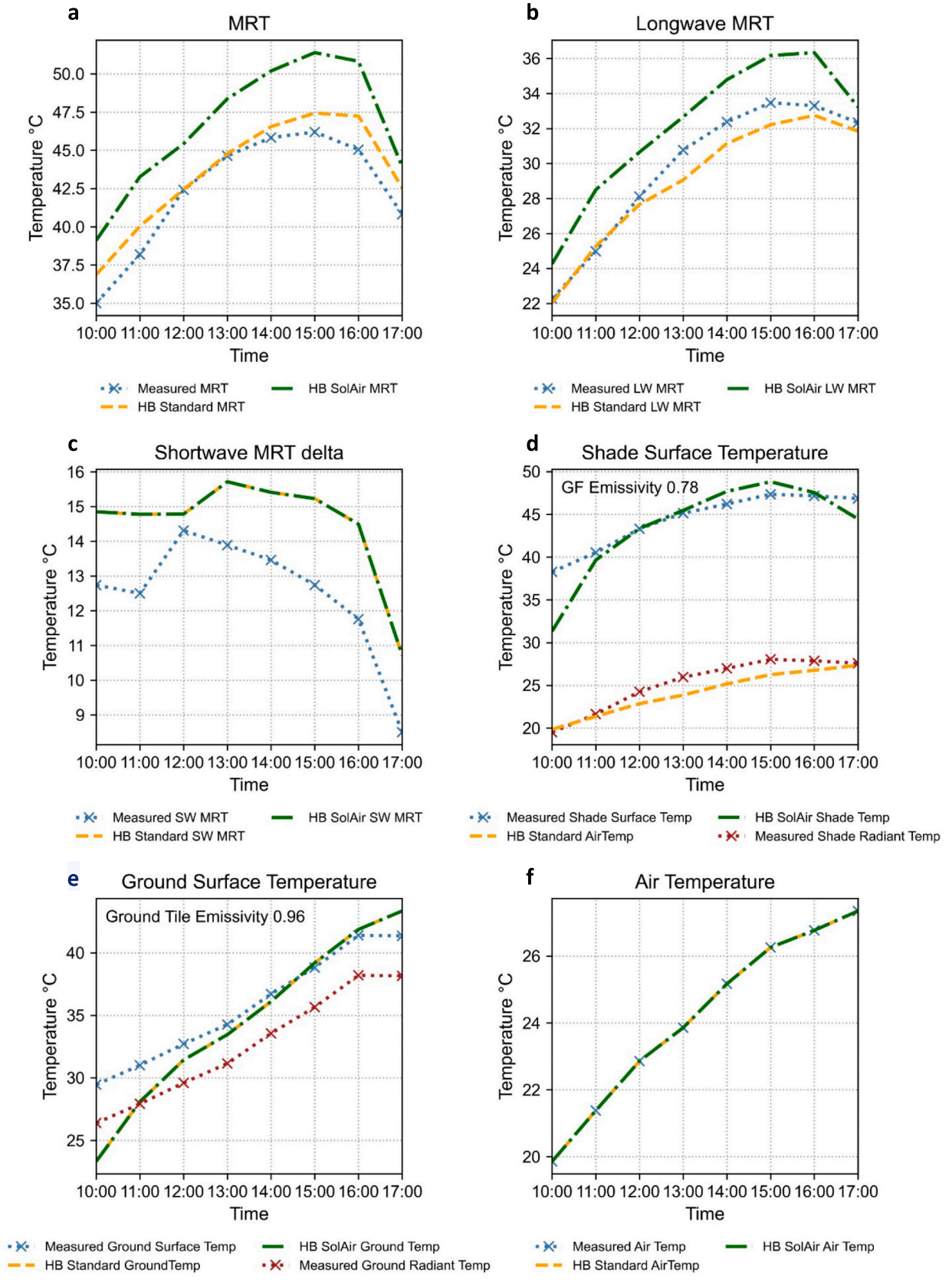

(caption on next page)

Fig. 7. **a)** to **f)** show time series plots comparing predicted data from Honeybee Standard (yellow) and SolAir (green) workflows with observed data (blue and red). **c)** The same SW MRT values are used for both workflows, since they share this stage of calculation **d)** Observed shade surface and radiant temperature are shown in comparison with the two workflows. The Standard workflow uses air temperature as shade temperature, since it is assumed to follow ambient temperatures. Material emissivity determines the conversion from radiant to surface temperature. **e)** and **f)** Ground and air temperatures were used for calibration only and are shown for reference.

coefficient calculated in step 2. The EPW air temperature was added to calculate the final shade surface temperature.

2.6.2.4. Step 4 Longwave mean radiant temperature. The LW MRT was calculated using a custom Python component based on HB Legacy code and adjusted to include surface emissivities and a LW delta (longwave exchange between person and sky. The base LW calculation weights surface temperatures with view factors from the sensor point to the respective surfaces. It also includes the emissivity of each surface and a normalization function since it is the ratios rather than absolute values that are relevant. The final

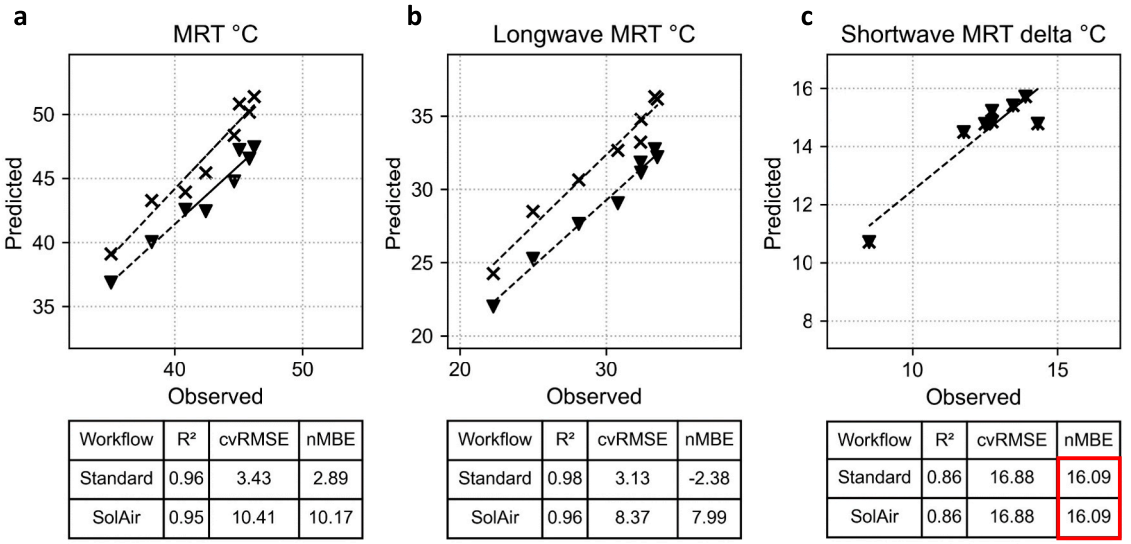

Workflow	R²	cvRMSE	nMBE
Standard	0.96	3.43	2.89
SolAir	0.95	10.41	10.17

Workflow	R²	cvRMSE	nMBE
Standard	0.98	3.13	-2.38
SolAir	0.96	8.37	7.99

Workflow	R²	cvRMSE	nMBE
Standard	0.86	16.88	16.09
SolAir	0.86	16.88	16.09

Workflow	R²	cvRMSE	nMBE
Standard	0.94	45.51	-45.46
SolAir	0.89	6.13	-1.84

Workflow	R²	cvRMSE	nMBE
Standard	0.97	7.22	-3.11
SolAir	0.97	7.22	-3.11

Workflow	R²	cvRMSE	nMBE
Standard	1.00	0.00	0.00
SolAir	1.00	0.00	0.00

Fig. 8. **a)** to **f)** show Scatter plots with R^2, nMBE and cvRMSE comparing agreement between predicted and observed data from Honeybee Standard workflow (▼) and SolAir workflow (×). Statistical measures above the ASHRAE threshold are highlighted in red, as seen in plots **c** and **d**. Plots **a** and **b** demonstrate good agreement for MRT and LW MRT for both workflows, with the statistical measures indicating the tendency for over or under estimation. Plots **e** and **f** display the calibration metrics, with predicted and observed ground surface temperatures showing very good agreement and air temperature corresponding between both workflows and the observed values.

Equation is shown in (Eq. (3)).

$$T_{mrt,lw} = \left(\sqrt[4]{\frac{\sum \epsilon_i F_i T_i^4}{\sum \epsilon_i F_i}} + 0.5 \bullet f_{svv} \bullet \left(T_{sky} - T_a \right) \right) - 273.15\ [C] \tag{3}$$

Where T_i is surface temperature (K), T_{sky} is sky temperature (K), T_a is air temperature (K), ε_i is surface emissivity, F_i is the surface view factor, and f_{svv} is the sky exposure, all unitless.

Ground surface temperature from the Standard workflow and shade surface temperature from the SolAir component were used, with user defined emissivity values. The view factors between the sensor point, surrounding surfaces and sky can be extracted from the UTCI component, but for the sake of simplicity were calculated through the LB View Percent component. This method is less refined because it provides a view factor to the entire surface rather than view factors corresponding to each face of the surface grid defined during the modelling process. However, it was considered suitable for the simple geometries used in this model. The final LW MRT is then added to the Standard workflow's SW MRT to calculate total MRT.

2.7. Data analysis

Once simulations were conducted, agreement between the measured and simulated temperatures were analysed through several statistical measures: The coefficient of determination (R^2), coefficient of variation of the Root Mean Square Error (cvRMSE) and normalized Mean Bias Error (nMBE). The ASHRAE Guidelines for energy model calibration (ASHRAE, 2014) recommend that for hourly data collection intervals the R^2 value should be over **0.75**, cvRMSE under **30%** and nMBE under **±10%.** These three measures indicate whether simulated temperatures follow the behaviour of the measured temperatures and if the model is over or under predicting temperatures on average.

3. Results & discussion: model validation

The following results first give a general summary of the validation of the two workflows for simulating MRT and proceed to an in-depth analysis and discussion of the two main errors seen in the models: the overestimation of SW MRT, and the significance of the inclusion of the shade surface temperature in the LW MRT calculations. A comparison of the two workflows is then given, before proceeding to Section 4 where the SolAir workflow is applied in a case study. Results from the field measurements are shown alongside the simulation results since their primary purpose was for validation of the model.

3.1. Validation of HB workflows

The results detailed in the following section are for the Honeybee workflows with resolved Radiance parameters of rflux|matrix, high accuracy and ambient bounces limited to 2. Time plot series of the simulated and measured data are provided for comparison in Fig. 7 and scatter plots showing model agreement are shown in Fig. 8. All components of the MRT calculation, except the SolAir nMBE which is on the edge of the threshold at 10.17%, and the nMBE of the SW MRT, at 16.09%, met the ASHRAE thresholds, showing good agreement between observed and predicted values. However, two main sources of error in the modelling workflow were evident – the effect of Radiance Parameters on the SW Delta, and the differences between the radiant temperature, surface temperature and how HB considers emissivity. These are discussed in the following paragraphs.

3.2. Shortwave mean radiant temperature delta

Results show the SW MRT delta was overestimated by up to 3 K in the simulation, and the nMBE was 6% over the ASHRAE threshold. Additionally, each simulation run produced a new SW MRT with variations up to 1 K, and peaks occurring at different times, within a four-hour range. While small differences are expected because of the stochastic method used by Radiance, the variation in peak times is more concerning. If ambient bounces are set to a higher and more accurate value such as 6, variation in values and peak times was reduced, but overestimation increased by up to 7 K.

Further investigation into this issue highlighted the high sensitivity of the SW MRT to the ground reflectivity: when the ground reflectivity was reduced from 0.30 to 0.15, and ambient bounces set to 6 the SW MRT was well below the ASHRAE thresholds with a R2 of 0.87, cvRMSE of 5.70% and nMBE of −0.80%. However, the predicted ground surface temperature was then overestimated by 10 K compared to observed temperatures. Errors either in the measurement of the ground surface temperature, or in determining the ground material properties during calibration, may have resulted in overestimation of the ground reflectivity and thus overestimation of the contribution of reflected radiation on SW MRT.

It is important to note the significance of the Radiance parameter, ambient bounces (−ab), which affects both the indirect and reflected radiation contribution on SW MRT. It is related to the number of ray bounces between surfaces, with an -ab of 0, for example, considering only direct radiation in the SW MRT calculation because it cuts off any ray bounces once the ray has 'found' a surface (Mardaljevic, 2011). In this study, the sensor was in open space but set between a ground surface and shade surface, meaning that it was receiving radiation reflected from the ground, interreflections between the ground and shade, indirect radiation from the sky, and a small amount of direct radiation from the shade surface. An -ab of 2, was found to provide predictions closest to observed values and is the minimum to consider an interreflection between ground and shade surface. On the other hand, Elrefai and Nikolopoulou (2023)

explicitly state the need to reduce ambient bounces to 1 to achieve a correlation between measurements and simulations for their sensors in direct sun in an urban canyon. An -ab of 1 considers one bounce between sensor and surface but excludes interreflections. This may indicate that HB is currently overestimating the indirect and reflected components of the SW MRT.

3.3. *Surface temperatures & longwave mean radiant temperature*

Though both workflows produced good agreement of LW MRT for this study, the differences between observed radiant and surface temperatures and predicted temperatures were investigated further to understand how they may produce error in more complex cases. The Standard workflow, which assumes a shade surface follows air temperature, was compared with the shade's observed radiant temperature, which is close to air temperature. The SolAir workflow was compared with the observed surface temperature, and both workflows shade temperature predictions are compared against the corresponding LW MRT. These comparisons are shown in Fig. 9.

The Standard workflow outperforms the SolAir workflow in LW MRT calculations, with an underestimation of just over 1 K compared to the SolAir workflow's overestimation of up to 4 K. In the Standard workflow, the shade surface is not included in the longwave exchange calculations for MRT, due to the assumption that it follows air temperature. However, the particular properties of the glassfibre, also result in a radiant temperature comparable with air temperature: its observed radiant temperature reaches a maximum of 3 K higher, despite the actual *surface* temperature reaching up to 20 K higher. Thus, while the Standard workflow excludes the shade surface in the calculation of LW MRT, there is only a small underestimation of LW MRT.

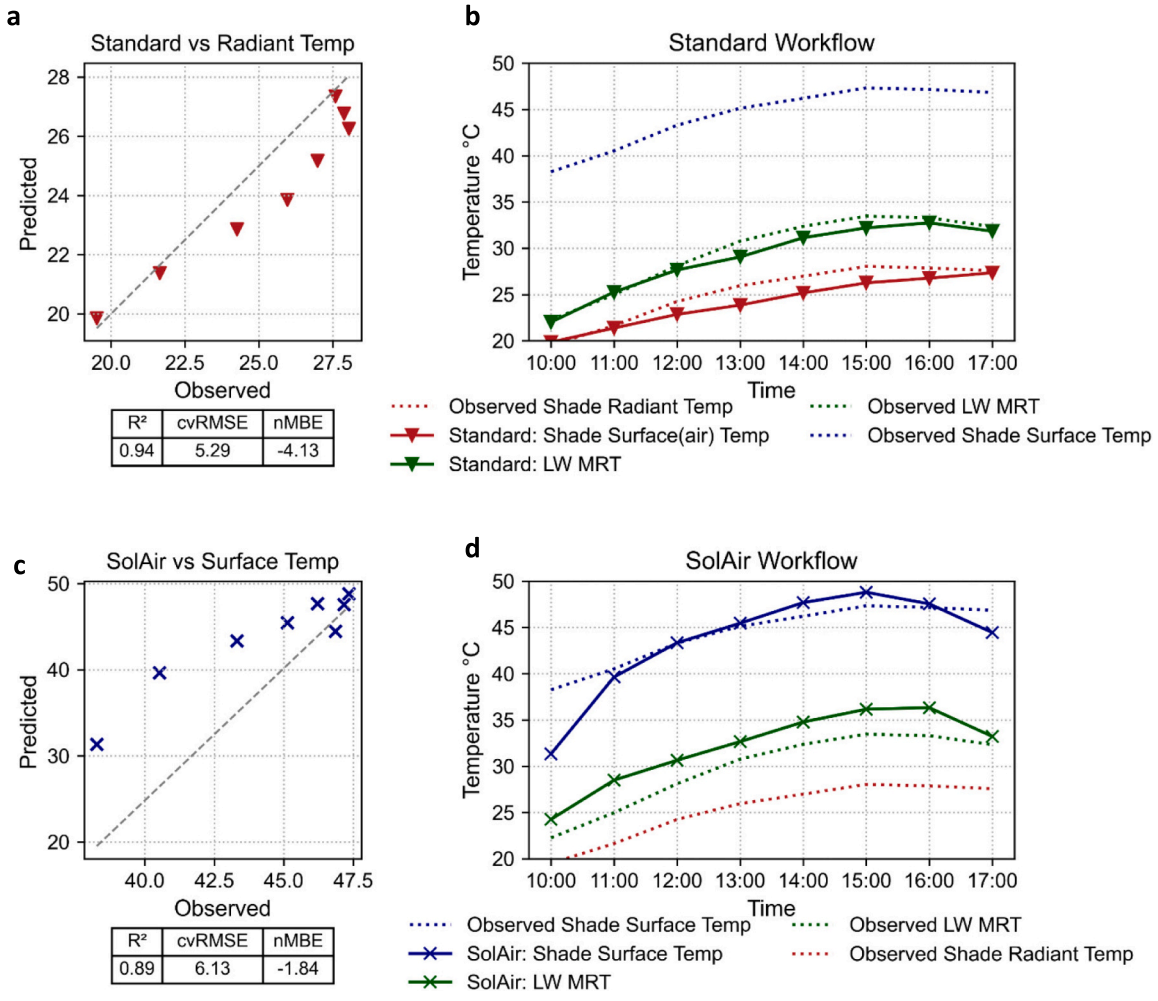

Fig. 9. The plots show the difference between the two workflows' approaches to modelling shade, and the correlation between the predicted shade temperatures, and LW MRT. **a)** Scatter plot and R^2, nMBE and cvRMSE showing the correlation between Standard workflow's shade surface temperature which is equivalent to air temperature, and the observed radiant temperature. **b**) Time series plot comparing predicted and observed longwave variables for Standard workflows: LW MRT and air temperature. Observed shade surface and radiant temperature are shown for comparison. **c)** Scatter plot and R^2, nMBE and cvRMSE showing the correlation between SolAir workflow's shade surface temperature and the observed surface temperature which is calculated from the radiant temperature through an emissivity correction factor. **d)** Time series plot comparing predicted and observed longwave variables for SolAir workflows: LW MRT and shade surface temperature.

In the SolAir model, a shade surface temperature is calculated and included in the LW MRT calculations. The SolAir shade surface temperature shows reasonable agreement with the actual observed glassfibre surface temperatures, but the approach results in a slightly overestimated LW MRT. Errors in the surface temperature calculation may be due to the assumptions made in the SolAir equations, where the textile is assumed to have no mass, and is opaque, whereas the glassfibre resembles a woven fabric with 10% openness factor, and heat storage capacity. The overestimation of LW MRT may be due to an error in the calculation of sky temperatures which is dependent on the Horizontal Infrared Radiation, the only boundary condition not measured on site and instead taken from the EPW file, or it may reflect the difference between Höppe's method of calculating MRT and the method used by E+ and consequently LBT. Each uses different weighting values for the calculation of the longwave radiation absorbed by the human body.

The maximum difference between the observed and predicted LW MRT is 1 K for the Standard workflow and 3 K for the SolAir workflow. Further work to clarify why the SolAir model overestimates LW MRT, and to understand the sensitivity of MRT to material thermal properties, such as the emissivity, will help determine where the SolAir workflow is most appropriate in design. Some standard shade materials such as cotton, high density polyethylene (HDPE) or polyvinyl chloride will tend to follow air temperature and have minimal effect on LW MRT due to properties such as high reflectivity, low heat capacity and relatively high emissivity values. However, Rossi et al. (2022) have shown that more innovative materials, such as aluminium gold foil, with an emissivity of 0.08, can lead to an increased cooling effect of up to 5.1 °C compared to a shade fabric with 0.87 emissivity. Additionally, shade devices made from materials with greater heat capacity will contribute to LW MRT and should be considered in microclimate simulations. Jareemit and Srivanit (2022) found warmer thermal conditions under a gray polycarbonate shade device compared to galvanized steel and HDPE, attributing this to the warmer surface temperatures reached by the polycarbonate.

3.4. LBT Validation conclusions

The study showed LBT to be a valid method of simulating MRT for the early-stage design process, where rapid feedback is essential. However, the biases and model limitations are important to be aware of. Specifically, in the Standard workflow, the exclusion of the freestanding shade from longwave calculations resulted in an underestimated LW MRT that masked the overestimation of SW MRT. The custom SolAir workflow was able to estimate the shade surface temperature within the ASHRAE thresholds but overestimated the LW MRT. In this case, the total error was magnified rather than masked.

The consequences for their application in design, means there is a probability of meaningful error when using the Standard workflow, if the radiant temperature of the shade surface is likely to diverge from air temperature, and is combined with low emissivity and a large view factor. It should also be assumed, that in both workflows, there will be an overestimation of SW MRT, though the reason for the error could not be confirmed. Ensuring correct Radiance parameters should minimize the variability in error however, if not the magnitude of error. Though more complex, the Sol-Air workflow will capture the effect of both material thermal and optical properties on MRT and therefore is more appropriate for studies into the performance of a shade material's thermal properties, understanding that there is bias to overestimate MRT. HB's UTCI Map component currently ignores Radiance's optical material characteristics, and therefore the SolAir workflow is also necessary if the designer wants to test the effect of optical properties such as translucency or selective reflection on thermal comfort.

The validation of both workflow is limited to one day, and to MRT alone. Further validation is needed during periods when longwave radiation dominates MRT, such as during nighttime hours, or when the model includes surrounding buildings. Additional work could include assessing the impact of shade devices on airflow by adding CFD analysis using Grasshopper plugins such as Eddy 3D (Kastner and Dogan, 2021). This would provide a more comprehensive understanding of the effect of lightweight shade on thermal comfort, although simulation time and complexity will increased. Further clarification of appropriate Radiance parameters for

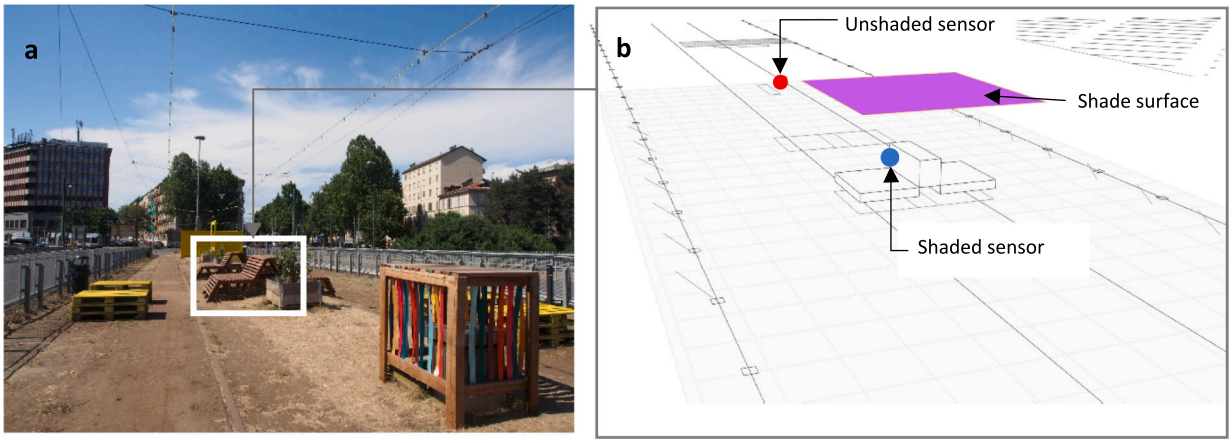

Fig. 10. **a)** the case study site at Precolinear Park in Turin marking the seating to be shaded in white and **b)** the corresponding CAD model drawn in Rhinoceros 8 and highlighting the test shade surface in purple. The position of the sensors points used in the simulations are also marked in red for unshaded and blue for shaded.

different scenarios and investigation into potential overestimation of reflections in the calculation of SW MRT is also recommended.

In the following section a case study on shade materials is conducted to evaluate the custom SolAir workflow's applicability in design.

4. Application in design

4.1. Precolinear park case study

The SolAir workflow was used in the design of street-scale temporary shading to for a small urban park in Turin, Italy. The urban park is a converted tram line, situated on a bridge crossing the river Po. As can be seen in Fig. 10a, the site is unshaded, but was used frequently for events and open-air exhibitions, particularly from mid-afternoon and throughout the evening. A simple shade canopy was considered for shading the wood bench seating, as highlighted in Fig. 10b, and simulations to test the effects of various design parameters on MRT were conducted using the SolAir workflow. The meteorological conditions of the simulation day are shown in Fig. 11, using air temperature, relative humidity and wind speed collected from a nearby weather station with uploaded data on the open source network (The Weather Company, 2023), and the radiation values collected from the Polito weather station.

4.2. Shade design parameters

The shade parameters tested were height, shade material and ground material. MRT has been shown to be sensitive to all three categories of parameters with Kántor, Chen and Gál et al. (2018) finding higher set shade sails providing a greater cooling effect then low set sails in their field studies. Similarly, Middel et al. (2021) observed significant differences in the magnitude of the cooling effect at different times of the day based on different combinations of shade material and ground surface.

The four materials tested were Glassfibre, Thin Film photovoltaic (PV), a standard white polyester PVC textile (PolyPVC) and an optimized high reflectivity-low emissivity foil (HighR/LowE). These are all examples of materials studied in outdoor thermal comfort studies (Pham et al., 2019; Rossi et al., 2022; Yuan et al., 2022). They are chosen to represent a range of optical and thermal properties that are currently used, or under development for use in the urban streetscape.

Because of the complexity of the thin film photovoltaic material (PV), surface temperature predictions using the SolAir workflow have been validated against field measurements, which can be found in Appendix Fig. C.1 along with validation of the surface temperature of the grass/soil construction. The observed data for both is based on previous field work described in (Nicholson et al., 2023). The PV is a multilayer material and is therefore modelled with an upper longwave emissivity/thermal absorption of 0.2 and lower face emissivity of 0.9 reflecting the difference between the solar cell and high-density polyethylene base in the field studies. It is also modelled as an inactive material, excluding the energy generated in calculation of surface temperatures. Table 4 gives the Shade and Ground material properties used in the HB simulations. Following the SolAir workflow described in Section 2.4, a ground zone was modelled with a 3x3m shade surface, and sensor placed at one meter directly underneath the shade. The person is represented as sitting, with emissivity of 0.95 and absorptivity of 0.7.

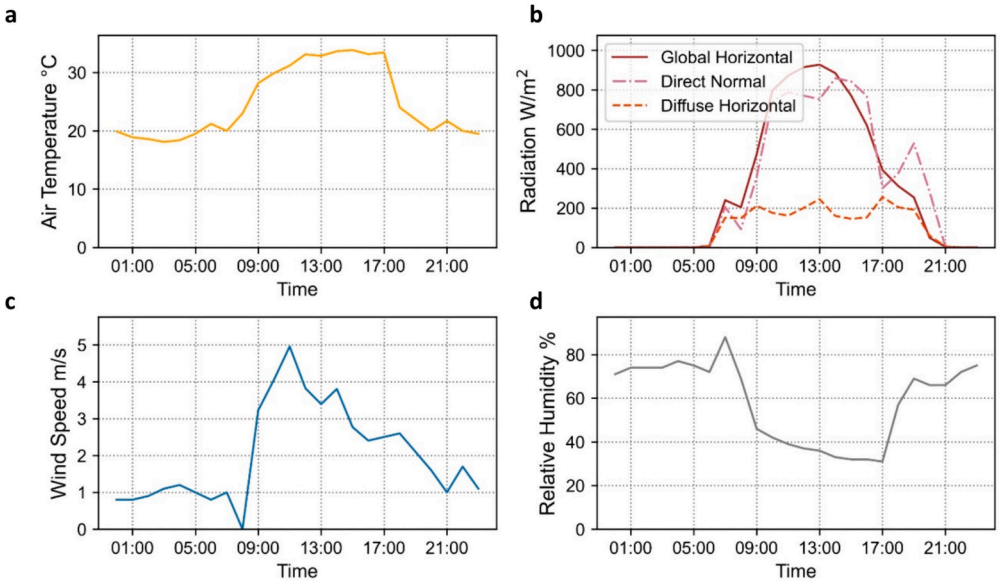

Fig. 11. Meteorological data for Precolinear Park, Turin, Italy for the 1st of July. **a)** Air temperature **c)**Wind Speed and **d)** relative humidity are provided by the open-source weather data network Wunderground, station i.d CorsoLanza - ITURIN3231 **b)** Radiation data is the same used in the validation studies and provided by Politecnico Di Torino measurements.

Table 4
Honeybee Material properties for Precolinear Park case study showing shade material properties for simulation of Glassfibre, Thin film photovoltaic, White polyester PVC and High Reflectivity/Low Emissivity Foil and ground material properties for simulating sparse grass.

Shade Material Properties	Glassfibre	Thin Film Photovoltaic	White Polyester PVC	High Reflectivity / Low Emissivity Foil
Transmittance	0.10	0.00	0.10	0.00
Roughness	Smooth	Very Smooth	Smooth	Very Smooth
Thermal Emissivity	0.78	Upper Layer: 0.20 Bottom Layer: 0.90	0.87	Upper Layer: 0.54 Bottom Layer: 0.08
Reflectivity	0.79	0.85	0.76	0.92

Ground Material Properties	**Grass/Soil**	**Concrete**
Thickness (m)	0.20	0.20
Conductivity (W/m-K)	3.00	1.73
Density (Kg/m^3)	1200	2243.0
Specific Heat Capacity (J/kg-K)	1252	837.0
Roughness	Rough	Medium Rough
Thermal Absorptance	0.92	0.90
Solar Absorptance	0.75	0.65
Visible Absorptance	0.75	0.65

4.3. Results & discussion

The simulation results are presented as time series plots (Fig. 12) and converted into matrices (Fig. 13) providing a generalized reference for determining the most effective shade parameters for the test location and period. Keeping in mind the errors discovered during the validation process, it is expected that there will be overestimations of MRT, due predominately to the overestimation of LW MRT from the SolAir workflow. If the overestimation of SW MRT was due to overweighting of reflected radiation by the simulation engine, rather than incorrect material properties or measurement error, the total overestimation of MRT may be up to 10%. Additionally, as the boundary conditions are set using data from outside the park, results are not expected to be as precise as those detailed in the validation section of this paper. However, as a comparative study, it is the relative differences rather than absolute values that are the important metric for designers.

4.3.1. Shade reflectivity, emissivity & transmissivity

The results show a clear and significant reduction in MRT for any form of shade, which can be attributed to their ability to block exposure to shortwave radiation. Between the four shade materials, there is a maximum of 16 K difference between the optimized material and thin film PV, minimal difference between the glassfibre and PolyPVC textiles, and a maximum of 10 K between the HighR/LowE material and the glassfibre and PolyPVC textiles. The differences between each indicate that both emissivity and reflectivity of the shade material play a role in thermal comfort, particularly where the surface is close to users as suggested in the literature. However, there is relatively low sensitivity, particularly for emissivity, with differences in the contribution to MRT only noticeable at very low emissivity values; for example, 0.08 for the HighR/LowE foil. The material transmittance also plays a role with the average cooling effect of the glassfibre and PolyPVC reducing to that below the PV from midday to afternoon, as shown in Fig. 12. This is most likely due to the 10% transmittance of the two textiles allowing more shortwave radiation to reach the person during the hours of the day where shortwave radiation is dominating thermal comfort.

4.3.2. Shade height vs time

The height of the shade appears to make a difference to the night-time cooling process, with the lower two heights leading to a gain in MRT between 20:00 to 6:00. These results should be interpreted with caution, since HB was not validated for the sunset to sunrise hours, where longwave energy fluxes dominate compared to daytime processes. However, it corresponds with the common trend noted in the literature (Aviv et al., 2021; Middel et al., 2021; Vartholomaios and Kalogirou, 2020). For design it implies the need to consider how shade height can balance a trade-off between daytime and night-time cooling, or whether the ability to move or open/close the shades at night should be included.

In all except the PV material, increasing the height of the shade reduces the duration of the cooling effect as well as, the maximum cooling effect. This is attributed to the higher shade no longer blocking the lower sun angles of this latitude. This trend contradicts the findings by Kàntor et al. (2018) that high set sails have a greater cooling effect, illustrating the significance of context in shade performance. Though both study sites shared similar latitudes and topographies, their measurements were conducted in a north-south canyon, with surrounding buildings able to block lower morning and afternoon sun angles. This study was conducted in open space, and thus exposed to all sun angles.

4.3.3. Shade height vs shade material

The cooling effect between materials becomes comparable as height increases, with only the HighR/LowE showing a noticeable difference from the other materials at 5 m. This suggests that it is the view factor, in combination with shade material properties, that should be considered in design. I.e. the material properties of an umbrella are more important considerations than those of a high

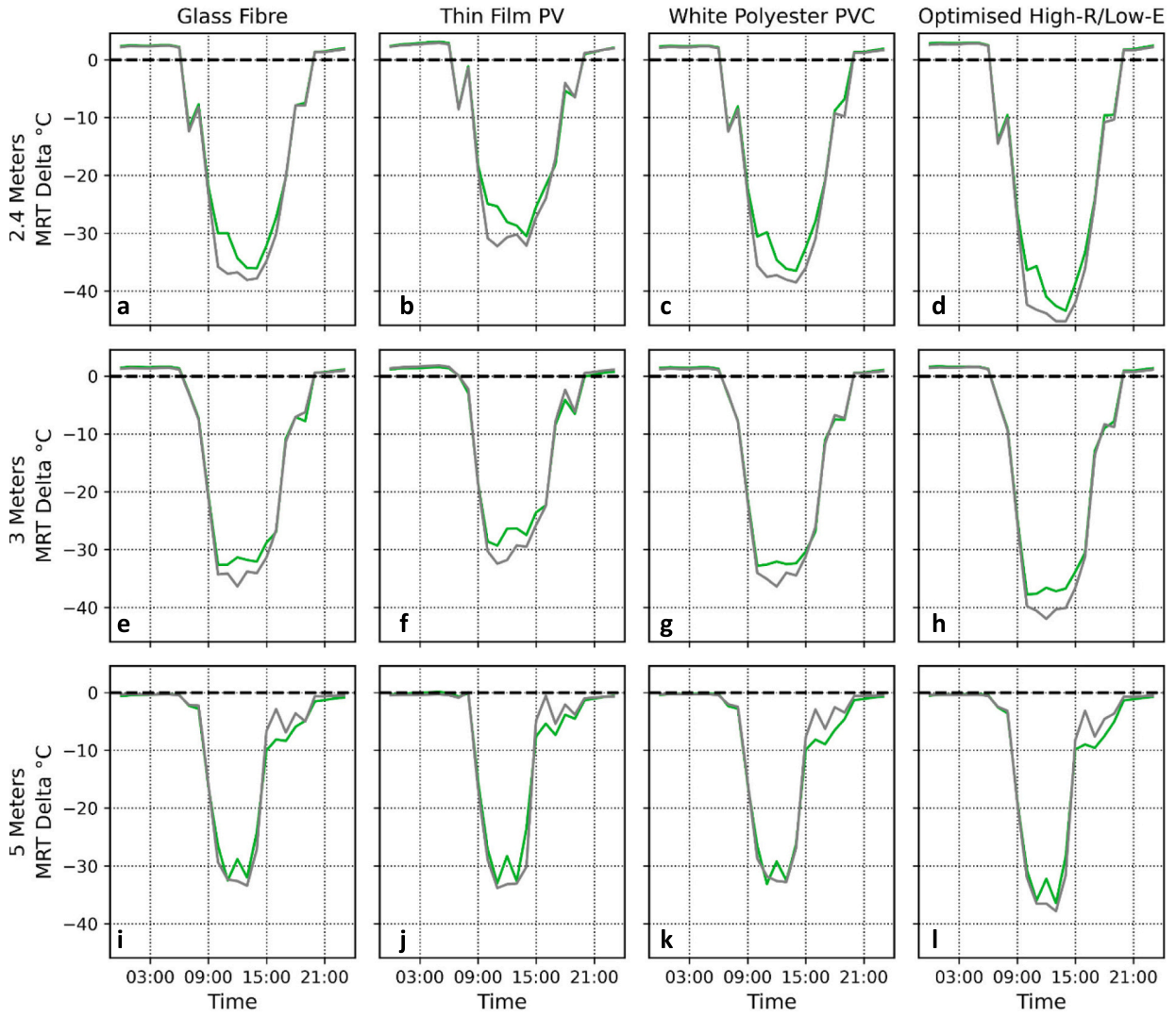

Fig. 12. a) to **l)** Change in MRT compared to unshaded person for combinations of shade heights, shade materials and ground materials for Precolinear park, Turin, Italy, 1st July. Green represents grass ground material and gray represents concrete pavement ground material. Plots **b, f** and **j** show the smallest cooling effect, and plots **d, h**, and **l** show the largest cooling effect. Moving vertically from plots **a, b, c d** to plots **i, j, k** and **l**, a reduction in the length of cooling period can be noted as well as reduced differences between shade material types.

mounted shade sail. In the case of the PV there is a slight reverse to the cooling trend decreasing with height, particularly at midday. This is due to the high temperatures reached by the PV, the effect of which only becomes negligible with the decreased view factor at 5 m. The results correspond to findings by Merchant et al. (2022) that overhead PV panels could have a reduced cooling effect when compared to other shade materials, and signifies the importance of considering thermal comfort in the introduction of photovoltaics into the streetscape. The most extreme change to reduction in MRT between heights is seen with the optimized material, most likely due it's very low emissivity, the effects of which become less significant with increasing height. In both the PV and High-R/Low-E the results suggest a relationship between emissivity, shade height (i.e. view factor) and MRT. This is a relationship discussed by Li et al. (2022) who noted the significant effect of ground longwave radiation on MRT, as a result of ground temperature, emissivity and view factor.

4.3.4. Ground material vs time

When considering the combined ground/shade performance, there was nearly a 20 K difference between the worst performing and best performing combinations: PV, 2.4 m, Grass/Soil and HighR/LowE, 2.4 m, Concrete, during the hottest periods of the day from 11:00 to 14:00. The better performance of the concrete over grass on average, is most likely due to the lower surface temperature resulting in part from the higher reflectivity. The lower sun angles during the afternoon shift the balance in favor of the grass with its lower reflectivity, since at these hours, the canopy was shading less of the ground surface, and reflected shortwave radiation from the ground began to have more effect on MRT. These findings appear to contradict those from Shashua-Bar et al. (2011) who noted the

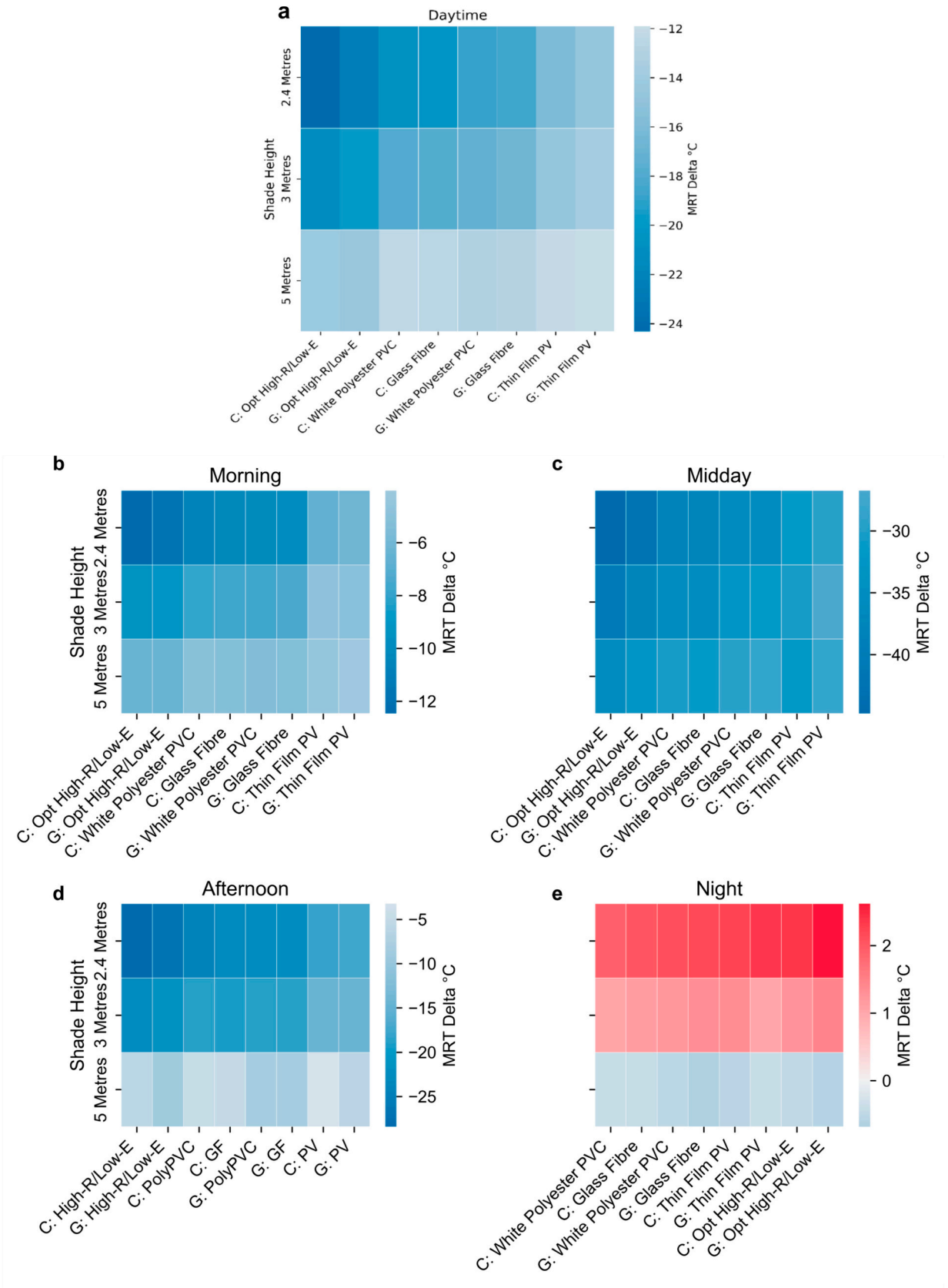

(caption on next page)

Fig. 13. Shade Design Matrices highlighting the most effective shade parameters, showing the average reduction in MRT compared to unshaded MRT for **a)** Daytime (5:00 to 20:00), **b)** Morning (6:00 to 9:00), **c)** Midday (12:00 to 14:00), **d)** Afternoon (15:00 to 18:00) and **e)** Night-time (21:00 to 4:00). C = Concrete and G = Grass/Soil.

superior cooling effect of grass over paving within a courtyard, however, this again can be imputed to the difference in context and is probably due to the courtyard walls providing shade during hours with lower sun angles, as well the differences in grass irrigation affecting surface temperature. It should be noted however that the results may be magnified due to the overestimation of SW MRT found in the validation section of this study.

The results provide valuable information on how various shade design parameters can affect thermal comfort. Focusing on the matrices in Fig. 12, provides the designer with options that allow them to balance other design aspects with that of optimized thermal comfort. At first glance the clear choice for shading at Precolinear Park is the high-R/low-E foil, at 2.4 m, over concrete. However, if considering the actual time of use of the space, from mid-afternoon to evening, the results indicate that the 5 m high shade canopy, over a grass/soil has similar or greater reduction in MRT. Additionally, grass/soil may be a preferable surface to concrete for a park, and a lower cost, or more readily available material such as the PolyPVC may be preferable.

4.3.5. Limitations of the workflow in design

Initial set-up of the SolAir workflow is relatively complex. It involves a significant number of steps in the modelling process, and requires knowledge on energy modelling, which is more common in engineering fields then design. Calibrating the EPW file with site specific data taken from online platforms also adds to the complexity. This interferes with the use of the tool in the design process. However, LBT is open source, meaning that once established, the workflow can be shared as a complete script, negating the need for others to build the workflows from scratch. Additionally, once the model is set up, individual parameters can be changed without repeating any data processing or modelling steps, helping to streamline the workflow.

Additional work to minimize simulation set-up time could include merging the calculation of the heat transfer coefficient and sol-air temperature and reducing the number of input variables by developing the Python code. Investigation into sensitivity of the model to different boundary conditions and methods for providing the meteorological data that balance accuracy with complexity are also opportunities for improving usability.

The workflow is limited to simple shade geometries and does not consider heat exchange with surrounding buildings because the SolAir component assumes form factors to the sky and ground are 1. This can lead to inaccuracies if the workflow is used in settings where there might be significant longwave gains from surrounding buildings, for example in street canyons where facades are exposed to the sun and of dark colors. It also limits exploration of the effect of shade form on LW MRT. Lightweight shading in practice is often curved, angled,or polyhedral, which can affect how sun angles are blocked, as well as longwave exchange between the surface and surrounds. Future work should include adding the calculation of form factors to the workflow to improve its applicability and provide a completely holistic method to predict the performance of free-standing shades.

4.3.6. Recommendations for use in shade design

Because LBT offers parametric simulation, users can expand the scope of their studies iteratively and increase the number of parameters studied to achieve the best possible response for the design problem. Using the workflows detailed in the paper, spatial and temporal aspects of MRT can be investigated further. For example, determining the specific sun angles a shade device needs to block, based on the surrounding shade context and use patterns of a location. In this case the Standard workflow may be used to support optimization of the shade structure and consequent form for the desired shade. One study merged LBT with an evolutionary solver to optimize the structure of a shade canopy based on minimizing direct solar radiation and canopy surface area, and maximizing sightlines from shade to surrounds (Van Ameijde et al., 2022). This study combined canopy and shade structure for a multifunctional analysis and could be expanded to optimize additional properties such as the canopy openness factor or reflectivity. Another application could include investigations into combinations of lightweight shade with other cooling strategies to increase overall thermal comfort. Palomo-Amores et al. (2023) show the combined use of temporary lightweight shading with tree shading can meet short-term and long-term thermal comfort needs, with the lightweight shading providing cooling while the shade trees mature. The Standard workflow described in this study could be used to identify where the lightweight shading should be located as the trees grow. Guo et al. (2023) discuss the need for high resolution shade planning to ensure a balance between openness and shade according to the types of urban space. In this instance the Standard workflow could be used to establish the location of shade devices, and the SolAir workflow to optimize the shade design.

5. Conclusion

While the importance of MRT is well established, this paper contributes to the understanding of the separate shortwave and longwave components of MRT resulting from lightweight shade devices in the urban streetscape. It also describes a novel workflow, using LBT, that can be used to design lightweight shading.

LBT's standard approach to modelling free standing shade was validated alongside a custom approach that considers the shade in longwave calculations. Both workflows can be considered appropriate for the early-stage design process where this parametric method of analysis is most valuable, and where the focus on comparative studies helps to mitigate the potential bias due to the overestimation errors discovered during the validation process. In their current versions, each are suited to specific applications: the Standard

workflow for shade spatial planning and designing shade form, and the SolAir workflow for material studies. To ensure reliable results in either workflow, the importance of correct material properties is highlighted as well as setting the appropriate Radiance parameters for the model. The Standard workflow is simpler to use but tends to overestimate SW MRT which is masked by the underestimation of LW MRT. The SolAir workflow requires further work to account for longwave exchanges between the shade and surrounding surfaces and allow modelling of more complex forms.

The SolAir workflow was used to investigate the effects of different shade materials on MRT, as well as the resulting effect on MRT due to interactions between shade and ground surfaces. The results highlighted the important role of material properties in outdoor thermal comfort, in combination with other design parameters such as low shade heights. Increasingly, engineered materials with selective wavelength absorption values, phase change materials and low-e materials are being developed. Understanding how these can perform in the urban environment will be important for heat mitigation. Further understanding of how more common materials can be optimized and adapted for local microclimates will also lead to improved outdoor urban space.

The study highlights the complexity of designing for thermal comfort and the value of detailed analysis and simulation tools in the design process. The use of LBT for developing the workflow is particularly valuable for designers because it makes it possible to investigate shade performance on a case by case basis leading to better adapted design for local microclimates. The workflows can be used to explore a wide range of parameters such as shade positioning, grouping of shades, slant, openness factor, translucency, shade support structures, and ground materials, all of which can be exploited for shade optimization. The ability to customize the modelling approach based on the design problem is an additional value, allowing designers to balance complexity with the needs for accuracy to facilitate data-driven design.

CRediT authorship contribution statement

Sinéad Nicholson: Writing – review & editing, Writing – original draft, Visualization, Validation, Software, Methodology, Investigation, Formal analysis, Data curation, Conceptualization. **Marialena Nikolopoulou:** Writing – review & editing, Supervision, Funding acquisition, Conceptualization. **Richard Watkins:** Writing – review & editing, Supervision, Methodology. **Monika Löve:** Supervision, Project administration. **Carlo Ratti:** Resources.

Declaration of generative AI and AI-assisted technologies in the writing process

During the preparation of this work the author(s) used ChatGPT 3.5/OpenAI in order to improve readability. After using this tool/service, the author(s) reviewed and edited the content as needed and take(s) full responsibility for the content of the publication.

Declaration of competing interest

Sinead Nicholson reports financial support was provided by European Commission Marie Sklodowska-Curie Actions. Sinead Nicholson reports equipment, drugs, or supplies was provided by Polytechnic of Turin. If there are other authors, they declare that they have no known competing financial interests or personal relationships that could have appeared to influence the work reported in this paper.

Data availability

Data will be made available on request.

Acknowledgements

This research is part of a project funded by the European Union's Horizon 2020 research and innovation programme under Marie SkłodowskaCurie grant agreement No. 861119.

Coleman Merchant and Forest Meggers from CHAOSLabs and Princeton University for their help in analyzing the high.RES sensor data, and Vincenzo Gentile & Marco Simonetti from the Department of Energy at the Polytechnic of Turin in providing research support and roof space for the field measurements and access to the Polytechnic of Turin's meteorological data.

Appendix A. Modelling Eqs

A.1. Honeybee calculation of MRT

Honeybee calculates MRT (Eq. (A.1)) from longwave components using Eq. (A.2) (U.S. Department of Energy, 2022a, b), and adds a SW delta derived from the SolCal method *(*Arens et al., 2015*)* (Eq. (A.3)). To adapt the equation for outdoor purposes HB adds a longwave delta (Eq. (A.4)) representing heat exchange with the sky and person. The shortwave component of the MRT equation performed by Honeybee uses solar radiation values taken from the EnergyPlus weather file (EPW) and Radiance to calculate the fractions of direct, indirect and reflected solar radiation reaching the sensor point through the modelled geometry. The amount absorbed by the human body, is defined by an additional component 'Solar Body Parameters' which sets user defined characteristics such as posture, skin color and clothing. The longwave components use Radiance to determine view factors between the sensor point

and to surrounding surfaces and the sky, E+ to simulate surface temperatures, and uses the air temperature and relative humidity or horizontal infrared values contained in the EPW file to calculate a sky temperature (Eq. (A.4)) (U.S. Department of Energy, 2022a, b, Section 5.1.3, p 197).

$$MRT = LW_{delta} + LW\,MRT + SW\,MRT\,[C] \tag{A.1}$$

$$LW\,MRT = \sqrt[4]{\sum F_i T_i^4} - 273.15[C] \tag{A.2}$$

Where

- T_i = Temperature of each surface [K]
- F_i = View factors to each surface

The SW delta is represented by:

$$ERF_{solar} = \left(0.5 \bullet f_{eff} \bullet f_{svv} \bullet \left(I_{diff} \bullet I_{th} \bullet R_{floor}\right) + A_p \bullet f_{bes} \bullet I_{dir} \bullet AD\right) \bullet \left(a_{sw} \bullet a_{lw}\right)\left[W/m^2\right] \tag{A.3}$$

Where:

- f_{eff} = fraction of the body that can radiate heat (related to posture)
- f_{svv} = sky view factor
- f_{bes} = fraction of body exposed to direct solar radiation
- I_{diff} = diffuse radiation [W/m^2]
- I_{th} =global horizontal radiation [W/m^2]
- I_{dir} = direct radiation [W/m^2]
- a_{sw} = short wave absorptivity of person (skin and clothing) default 0.7
- a_{lw} = long wave absorptivity/emissivity (clothing) default 0.95
- R_{floor} = ground reflectance
- h_r = radiant heat transfer coefficient
- A_p / AD = projection factor determined through a look up table available at ASHRAE and is determined by solar altitude, solar azimuth and the body's related angle.
- T_a= Dry bulb temperature K

The longwave delta LW_{delta} is calculated by:

$$0.5 \bullet f_{svv} \bullet \left(T_{sky} - T_a\right) - 273.15\,[^{\circ}\mathrm{c}] \tag{A.4}$$

Where:

- f_{svv} is the view factor calculated using HB View Factor Component
- T_{sky} is sky temperature
- T_a is air temperature taken from the EPW file

And

$$T_{sky} = \sqrt[4]{\frac{L_a}{\sigma \bullet \epsilon}}[K] \tag{A.5}$$

Where:

- L_a (W/m^2) is the horizontal infrared radiation taken from the EPW file
- σ Is the Stefan-Bolztmann constant (5.667 $\times$ 10^{-8}) [W/m^2 K^4]
- ϵ is source emissivity (0.95 for person)

A.2. Equations for SolAir (O'Callaghan and Probert, 1977).

$$T_{sol-air} = T_o + \frac{a \bullet I - \Delta Q_{ir}}{h_o}[C] \tag{A.6}$$

Where:
Q_{lw} (Longwave Radiation Flux (U.S. Department of Energy, 2022a, b, Section 3.5.2, pg 90*).*

$$\Delta Q_{ir} = \epsilon\sigma F_{sky}\left(T^4_{ambient} - T^4_{sky)} + \epsilon\sigma F_{ground}\left(T^4_{ambient} - T^4_{ground)}\right)\left[W/m^2\right] \tag{A.7}$$

- σ = the Stefan-Bolztmann constant
- ϵ = the surface emissivity
- $T_{ambient}$ = dry bulb temperature [K], representing the shade surface temperature
- T_{sky} = sky temperature [K]
- F_{sky} = view factor from shade surface to sky temperature
- T_{ground} = ground temperature [K]
- F_{ground} = view factor from shade surface to ground temperature

h_o *(Heat Transfer Coefficient) using the SIMPLE Combined algorithm* (U.S. Department of Energy, 2022a, b, Section 3.5.5.1, pg. 96).

$$h_o = D + EVz + FVz\ 2\ \left[W/m^2K\right] \tag{A.8}$$

- V = local wind speed calculated at the height above ground of the surface centroid [m/s]
  D, E, F = material roughness coefficients.

Qsw (Shortwave Radiation Flux).

$$Qsw = a \bullet t \bullet I_{up} + a \bullet I_{down}\left[W/m^2\right] \tag{A.9}$$

- a = surface solar absorption
- t = surface transmittance
- I_{up}= global solar irradiance, upwards sensors [W/m^2]
- I_{down} = global solar irradiance, downwards sensors (W/m^2)

Appendix B. SolAir Python code

B.1. Heat transfer coefficient

```python
__author__ = "sinead"
__version__ = "2024.02.14"

# Input parameters
roughness = material_roughness # Assign roughness input from Grasshopper
wind_speeds = hourly_wind_speeds # Assign wind speeds input from EPW

def calc_htc(wind_speeds, material_coefficients, roughness):
    htc = []
    coefficients = material_coefficients.get(roughness, [0, 0, 0])
    D, E, F = coefficients
    for ws in wind_speeds:
        h = D + E * ws + F * ws ** 2
        htc.append(h)
    return htc

material_coefficients = {
    "VerySmooth": [8.23, 3.33, -0.036],
    "Smooth": [10.22, 3.10, 0.00],
    "MediumSmooth": [8.23, 4.00, -0.057],
    "MediumRough": [10.79, 4.192, 0.0],
}

# Calculate heat transfer coefficient
hourly_htc = calc_htc(wind_speeds, material_coefficients, roughness)
```

B.2. SolAir temperature

```
__author__ = "sinead"
__version__ = "2024.02.14"

from ladybug_rhino.grasshopper import all_required_inputs
import math

"""
    Args:
        Horiz_ir_rad: Hourly horizontal Infrared Radiation (W/m2) data from imported EPW.
        incident_radiation: List of houlry incident radiation values from HB UTCI Comfort Map
or HB annual Irradiance

        reflected_radiation: List of hourly reflected radiation values from HB UTCI Comfort Map
or HB Annual Irradiance
        Dry_bulb: Hourly dry bulb temperature (C) from imported EPW.
        emissivity_top: Shade surface upper material's emissivity value.
        emissivity_bottom: Shade surface lower material's emissivity value.
        reflectivity_top: Material's top layer reflectivity value.
        reflectivity_bottom: Material's bottom layer reflectivity value.
        transmittance: Shade surface material's transmittance value.
        Ground_temp: List of hourly ground surface temperatures (C) from field measurements or
HB UTCI Comfort Map. Can also use dry bulb from EPW if ground temperatures aren't available.
        HTC: Hourly heat transfer coefficient calculated from SimpleCombined Method
    Returns:
        Sky_Temp: Calculated hourly sky temperature values (C)
        Qsw: List of calculated hourly shortwave flux values (W)
        Qlw: List of calculated hourly longwave flux values (W)
        SolAirTemp: List of calculated hourly shade surface temperature values (C)
"""

# Default constants
sigma = 5.6697e-8
F = 1

# Input parameters
La = Horiz_ir_rad
Ta_celsius = Dry_bulb
Tg_celsius = Ground_Temp
e_top = emissivity_top
e_bottom = emissivity_bottom
I = incident_radiation
I_r = reflected_radiation
t = transmittance
r1 = reflectivity_top
r2 = reflectivity_bottom
HTC = HTC
_run = _run

# Convert Celsius to Kelvin
Ta = [temp_celsius + 273.15 for temp_celsius in Ta_celsius]
Tg = [temp_celsius + 273.15 for temp_celsius in Tg_celsius]

# Define function to calculate sky temperature
def calc_sky_temp():
    return [(La_val /sigma) ** 0.25 for La_val in La]

# Define function to calculate longwave radiation heat transfer
def calc_Qlw(T, Tsurf, e, F):
    return [e * sigma * F * ((Tsurf_val ** 4) - (T_val ** 4)) for T_val, Tsurf_val in zip(T,
Tsurf)]

# Define function to calculate shortwave radiation flux
def calc_Qsw():
    return [(I_val * (1 - (t + r1))) + (I_r_val * (1- (r2))) for I_val, I_r_val in zip(I, I_r)]

# Define function to calculate sol-air temperature
def calc_Tsolair():
    return [Ta_val + ((hourly_Qsw_val - total_Qlw_val) / HTC_val) for Ta_val, hourly_Qsw_val,
total_Qlw_val, HTC_val in zip(Ta_celsius, hourly_Qsw, total_Qlw, HTC)]

#Define function to convert temperatures from kelvin to celsius
def kelvin_to_celsius(temp_kelvin):
    return temp_kelvin - 273.15
```

```
# Calculate Sky Temperature
Tsky = calc_sky_temp()
Tsky_celsius = [kelvin_to_celsius(temp_kelvin) for temp_kelvin in Tsky]

# Calculate longwave fluxes (W/m2)
hourly_Qlw_sky = calc_Qlw(Tsky, Ta, e_top, F)
hourly_Qlw_ground = calc_Qlw(Tg, Ta, e_bottom, F)
total_Qlw = [sky + ground for sky, ground in zip(hourly_Qlw_sky, hourly_Qlw_ground)]

# Calculate shortwave fluxes (W/m2)
hourly_Qsw = calc_Qsw()

# Calculate Tsol-air
if all_required_inputs(ghenv.Component) and _run:
    Tsolair = calc_Tsolair()

# Output
Sky_Temp = Tsky_celsius
Qsw = hourly_Qsw
Qlw = total_Qlw
SolAirTemp = Tsolair
```

. (*continued*).

B.3. Longwave mean radiant temperature

```
__author__ = "sinead"
__version__ = "2024.01.27"

import math
from Grasshopper import DataTree
from Grasshopper.Kernel.Data import GH_Path
from ladybug_rhino.grasshopper import all_required_inputs

"""
    Args:
        sky_temp: List of hourly calculated sky temperatures (C)from SolAir or UTCI Comfort Map
        ambient_temp: List of hourly average of surrounding surface temperatures or dry bulb
temperature from EPW (C)
        sky_exposure: Sky exposure value from sensor point to sky from UTCI Comfort Map or LB
View Percent
        temperatures: Data tree containing lists of hourly surface temperatures (C)
        viewFactors: List of view factors corresponding to the respective surface temperature
branch from the temperature data tree
        emissivities: List of emissivities corresponding to the respective surface temperature
branch from the temperature data tree
    Returns:
        Lw_delta: List of calculated hourly longwave delta (C)
        Base_mrt: List of calculated hourly longwave mrt values without the longwave delta
        Lw_MRT: List of calculated hourly sum of base_mrt and longwave delta ©

"""

def longwave_mrt_delta_from_sky_temp(sky_temp, ambient_temp, sky_exposure):
    lw_delta = []
    for i in range(min(len(sky_temp), len(ambient_temp))):
        sky_temp_K = sky_temp[i] + 273.15
        ambient_temp_K = ambient_temp[i] + 273.15
        result = 0.5 * sky_exposure * (sky_temp_K - ambient_temp_K)
        lw_delta.append(result)
    return lw_delta

def getMRT(temperatures, viewFactors, emissivities):
    equRight = 0
    sum_view_emiss = sum(viewFactors[i] * emissivities[i] for i in range(len(viewFactors)))

    for i, temp in enumerate(temperatures):
        tempK = temp + 273.15
        equRight = equRight + math.pow(tempK, 4) * viewFactors[i] * emissivities[i]
    MRT = math.pow(equRight/sum_view_emiss, 0.25)
    MRTC = MRT - 273.15
    return MRTC

def main(temperatures, viewFactors, emissivities):
    #Create a Python list from the temperature data tree.
    dataPyList = []
    for i in range(temperatures.BranchCount):
        branchList = temperatures.Branch(i)
        dataVal = []
        for item in branchList:
            try: dataVal.append(float(item))
            except: dataVal.append(item)
        dataPyList.append(dataVal)

    MRTs = DataTree[object]()
    for count, templist in enumerate(dataPyList):
        mrt = getMRT(templist, viewFactors, emissivities)
        p = GH_Path(count)
        MRTs.Add(mrt, p)

    return MRTs

if all_required_inputs(ghenv.Component) and _run is True:
    lw_dmrt = longwave_mrt_delta_from_sky_temp(sky_temp, ambient_temp, sky_exposure)

if temperatures.BranchCount >0 and viewFactors != [] and viewFactors != [None] and emissivities
!= [] and emissivities != [None]:
    base_mrt = main(temperatures, viewFactors, emissivities)

base_mrt_list = [base_mrt.Branch(i)[0] for i in range(base_mrt.BranchCount)]
lw_mrt = [delta + base for delta, base in zip(lw_dmrt, base_mrt_list)]
```

Appendix C. Appendix

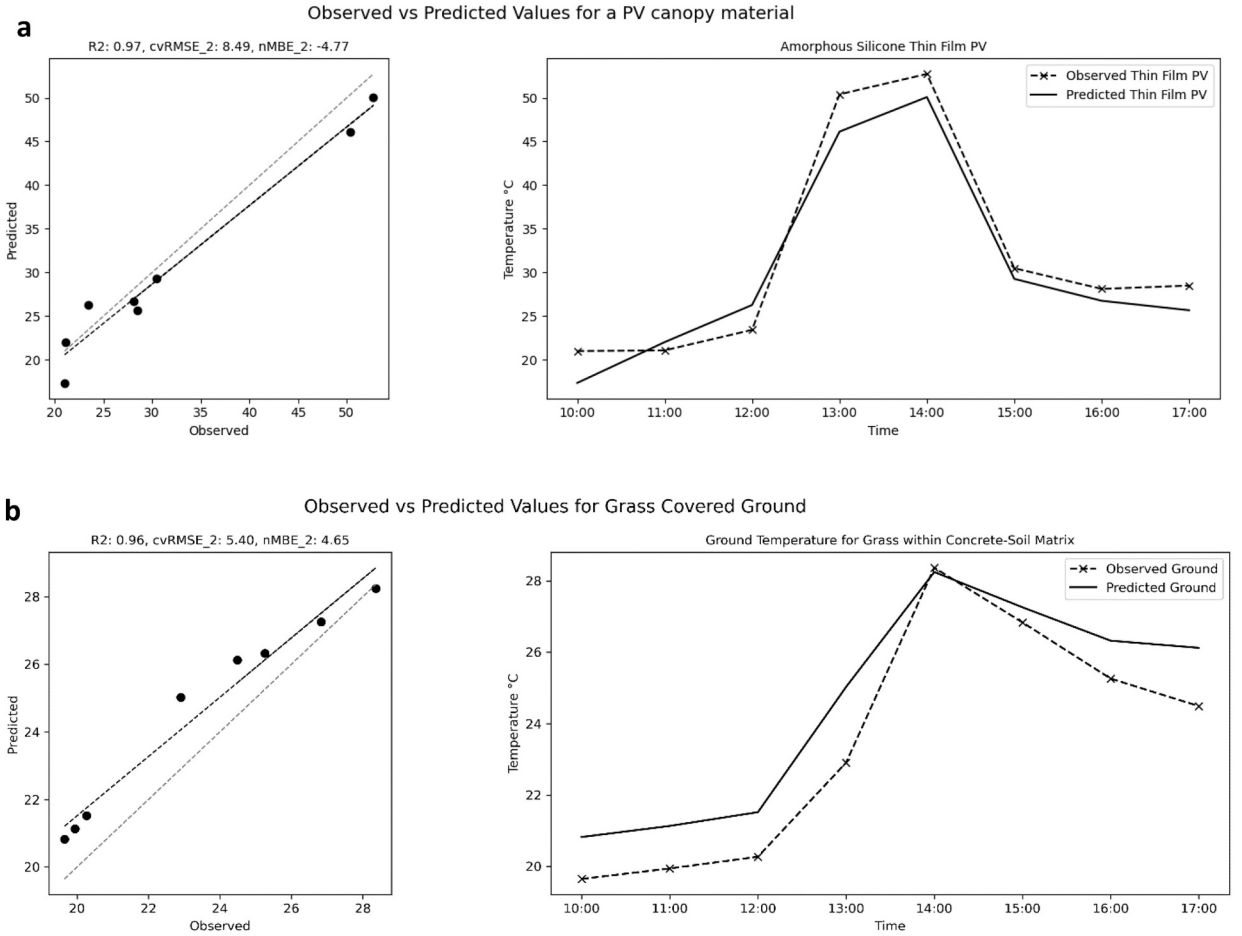

Fig. C.1. Scatter and time series plots comparing observed and predicted surface temperatures for **a)** an (inactive) thin film amorphous silicon photovoltaic parasol and **b)** grass ground material. Observations were taken 19th September 2021, in Turin, Italy (45°09′N, 7°66′E) (See Nicholson et al., 2023).

References

Alharthi, M., Sharples, S., 2020. Modelling and testing extendable shading devices to mitigate thermal discomfort in a hot arid climate: a case study for the hajj in Makkah, Saudi Arabia. In: Rodríguez-Álvarez, J., Soares Goncalves, J.C. (Eds.), Planning Post Carbon Cities, Vol. 1. University of A Coruña, pp. 654–659. https://doi.org/10.17979/spudc.9788497497947.

Arens, E., Hoyt, T., Zhou, X., Huang, L., Zhang, H., Schiavon, S., 2015. Modeling the Comfort Effects of Short-Wave Solar Radiation Indoors. https://doi.org/10.1016/j.buildenv.2014.09.004.

Armson, D., Asrafur Rahman, M., Roland Ennos, A., 2013. A comparison of the shading effectiveness of five different street tree species in Manchester, UK. Arboricult. Urban For. 39 (4) https://doi.org/10.48044/jauf.2013.021.

ASHRAE ASHRAE Guideline 14–2014: Measurement of Energy, Demand, and Water Savings (Version 2014). (2014). [Guideline 14]. chrome-extension://efaidnbmnnnibpcajpcglclefindmkaj/https://upgreengrade.ir/admin_panel/assets/images/books/ASHRAE%20Guideline%2014-2014.pdf.

Aviv, D., Guo, H., Middel, A., Meggers, F., 2021. Evaluating radiant heat in an outdoor urban environment: resolving spatial and temporal variations with two sensing platforms and data-driven simulation. Urban Clim. 35, 100745 https://doi.org/10.1016/j.uclim.2020.100745.

Bruse, M., 2004. ENVI-met 3.0: Updated Model Overview.

Calabrò, E., Meggers, F., Teitelbaum, E., Guo, H., Gmachl, C., Penello, G.M., 2015. Thermoheliodome testing: evaluation methods for testing directed radiant heat reflection. Energy Procedia 78, 1762–1768. https://doi.org/10.1016/j.egypro.2015.11.298.

Carleton, T.A., Jina, A., Delgado, M.T., Greenstone, M., Houser, T., Hsiang, S.M., Hultgren, A., Kopp, R.E., 2020. Valuing the Global Mortality Consequences of Climate Change Accounting for Adaptation Costs and Benefits (Working Paper Series). National Bureau of Economic Research, p. 56. https://doi.org/10.3386/w27599.

Castellani, B., 2021. Application of retro-reflective materials in urban canyon at different geographical locations. Build. Environ. 193, 107676 https://doi.org/10.1016/j.buildenv.2021.107676.

Chi, D.A., González, M., E., Valdivia, R., & Gutiérrez J., E., 2021. Parametric design and comfort optimization of dynamic shading structures. Sustainability 13 (14), 7670. https://doi.org/10.3390/su13147670.

Chiang, Y.-C., Li, D., Jane, H.-A., 2017. Wild or tended nature? The effects of landscape location and vegetation density on physiological and psychological responses. Landsc. Urban Plan. 167, 72–83. https://doi.org/10.1016/j.landurbplan.2017.06.001.
Colter, K.R., Middel, A.C., Martin, C.A., 2019a. Effects of natural and artificial shade on human thermal comfort in residential neighborhood parks of Phoenix, Arizona, USA. Urban For. Urban Green. 44, 126429 https://doi.org/10.1016/j.ufug.2019.126429.
Colter, K.R., Middel, A.C., Martin, C.A., 2019b. Effects of natural and artificial shade on human thermal comfort in residential neighborhood parks of Phoenix, Arizona, USA. Urban For. Urban Green. 44, 126429 https://doi.org/10.1016/j.ufug.2019.126429.
Cortesão, J., Alves, F.B., Patterson, J., 2013. Thermal Retrofitting of Public Spaces in Compact Urban Areas. A Bioclimatic Approach. University of Porto.
Coutts, A.M., White, E.C., Tapper, N.J., Beringer, J., Livesley, S.J., 2016. Temperature and human thermal comfort effects of street trees across three contrasting street canyon environments. Theor. Appl. Climatol. 124 (1–2), 55–68. https://doi.org/10.1007/s00704-015-1409-y.
CustomWeather, 2021. Past Weather in Turin, Italy—Yesterday or Further Back. https://www.timeanddate.com/weather/italy/turin/historic.
Elgheznawy, D., Eltarabily, S., 2021. The impact of sun sail-shading strategy on the thermal comfort in school courtyards. Build. Environ. 202, 108046 https://doi.org/10.1016/j.buildenv.2021.108046.
Elrefai, R., Nikolopoulou, M., 2023. A simplified outdoor shading assessment method (OSAM) to identify outdoor shading requirements over the year within an urban context. Sustain. Cities Soc. 97, 104773 https://doi.org/10.1016/j.scs.2023.104773.
Elwy, I., Ibrahim, Y., Fahmy, M., Mahdy, M., 2018. Outdoor microclimatic validation for hybrid simulation workflow in hot arid climates against ENVI-met and field measurements. Energy Procedia 153, 29–34. https://doi.org/10.1016/j.egypro.2018.10.009.
Emmanuel, R., Rosenlund, H., Johansson, E., 2007. Urban shading—a design option for the tropics? A study in Colombo, Sri Lanka. Int. J. Climatol. 27 (14), 1995–2004. https://doi.org/10.1002/joc.1609.
Erell, E., Pearlmutter, D., Williamson, T., 2011. June 23 (Urban Microclimate– Designing the Spaces Between Buildings).
Erell, E., Pearlmutter, D., Boneh, D., Kutiel, P.B., 2014. Effect of high-albedo materials on pedestrian heat stress in urban street canyons. Urban Clim. 10, 367–386. https://doi.org/10.1016/j.uclim.2013.10.005.
Ettinger, A.K., Bratman, G.N., Carey, M., Hebert, R., Hill, O., Kett, H., Levin, P., Murphy-Williams, M., Wyse, L., 2024. Street trees provide an opportunity to mitigate urban heat and reduce risk of high heat exposure. Sci. Rep. 14 (1), 3266. https://doi.org/10.1038/s41598-024-51921-y.
Evola, G., Costanzo, V., Magrì, C., Margani, G., Marletta, L., Naboni, E., 2020. A novel comprehensive workflow for modelling outdoor thermal comfort and energy demand in urban canyons: results and critical issues. Energ. Build. 216, 109946 https://doi.org/10.1016/j.enbuild.2020.109946.
Francis, J., Giles-Corti, B., Wood, L., Knuiman, M., 2012. Creating sense of community: the role of public space. J. Environ. Psychol. 32 (4), 401–409. https://doi.org/10.1016/j.jenvp.2012.07.002.
Garcia-Nevado, E., Beckers, B., Coch, H., 2020. Assessing the cooling effect of urban textile shading devices through time-lapse thermography. Sustainable Cities and Society 63, 102458. https://doi.org/10.1016/j.scs.2020.102458.
Greg Ward, 2021. Radiance (5.4a) [C; Windows]. https://www.radiance-online.org/.
Guo, F., Guo, R., Zhang, H., Dong, J., Zhao, J., 2023. A canopy shading-based approach to heat exposure risk mitigation in small squares. Urban Clim. 49, 101495 https://doi.org/10.1016/j.uclim.2023.101495.
Harlan, S.L., Brazel, A.J., Jenerette, G.D., Jones, N.S., Larsen, L., Prashad, L., Stefanov, W.L., 2007. In the shade of affluence: The inequitable distribution of the urban heat island. In: Research in Social Problems and Public Policy, Vol. 15. Emerald (MCB UP), pp. 173–202. https://doi.org/10.1016/S0196-1152(07)15005-5.
Höppe, P., 1992. A new procedure to determine the mean radiant temperature outdoors. Wetter Und Leben 44, 147–151.
Höppe, P., 1999. The physiological equivalent temperature—A universal index for the biometeorological assessment of the thermal environment. Int. J. Biometeorol. 43 (2), 71–75. https://doi.org/10.1007/s004840050118.
Ibrahim, Y., Kershaw, T., Shepherd, P., 2020. Improvement of the Ladybug-Tools Microclimate Workflow: A Verification Study.
Jareemit, D., Srivanit, M., 2022. A comparative study of cooling performance and thermal comfort under street market shades and tree canopies in tropical savanna climate. Sustainability 14 (8), 4653. https://doi.org/10.3390/su14084653.
Jendritzky, G., De Dear, R., Havenith, G., 2012. UTCI—why another thermal index? Int. J. Biometeorol. 56 (3), 421–428. https://doi.org/10.1007/s00484-011-0513-7.
Johansson, E., Thorsson, S., Emmanuel, R., Krüger, E., 2014. Instruments and methods in outdoor thermal comfort studies – the need for standardization. Urban Clim. 10, 346–366. https://doi.org/10.1016/j.uclim.2013.12.002.
Kántor, N., Unger, J., 2011. The most problematic variable in the course of human-biometeorological comfort assessment—the mean radiant temperature. Open Geosci. 3 (1), 90–100. https://doi.org/10.2478/s13533-011-0010-x.
Kántor, N., Chen, L., Gál, C.V., 2018. Human-biometeorological significance of shading in urban public spaces—summertime measurements in Pécs, Hungary. Landsc. Urban Plan. 170, 241–255. https://doi.org/10.1016/j.landurbplan.2017.09.030.
Kastner, P., Dogan, T., 2021. Eddy 3D: A toolkit for decoupled outdoor thermal comfort simulations in urban areas. Build. Environ., 108639 https://doi.org/10.1016/j.buildenv.2021.108639.
Kottek, M., Grieser, J., Beck, C., Rudolf, B., Rubel, F., 2006. World map of the Köppen-Geiger climate classification updated. Meteorol. Z. 15 (3), 259–263. https://doi.org/10.1127/0941-2948/2006/0130.
Lee, I., Voogt, J., Gillespie, T., 2018. Analysis and comparison of shading strategies to increase human thermal comfort in urban areas. Atmosphere 9 (3), 91. https://doi.org/10.3390/atmos9030091.
Li, Z., Feng, X., Chen, W., Fang, Z., 2022. Quantifying the effect of ground view factor and ground temperature on outdoor mean radiant temperature. Sustain. Cities Soc. 84, 104030 https://doi.org/10.1016/j.scs.2022.104030.
Lindberg, F., Holmer, B., Thorsson, S., 2008. SOLWEIG 1.0 – modelling spatial variations of 3D radiant fluxes and mean radiant temperature in complex urban settings. Int. J. Biometeorol. 52 (7), 697–713. https://doi.org/10.1007/s00484-008-0162-7.
López-Cabeza, V.P., Diz-Mellado, E., Rivera-Gómez, C., Galán-Marín, C., Samuelson, H.W., 2022. Thermal comfort modelling and empirical validation of predicted air temperature in hot-summer Mediterranean courtyards. J. Build. Perform. Simul. 15 (1), 39–61. https://doi.org/10.1080/19401493.2021.2001571.
Lucarelli, C.D.C., Carlo, J.C., 2020. Parametric modeling simulation for an origami shaped canopy. Front. Architect. Res. 9 (1), 67–81. https://doi.org/10.1016/j.foar.2019.08.001.
Chris Mackey. (2016a). Trees in Outdoor Thermal Comfort (Code Example) [Computer Software]. http://hydrashare.github.io/hydra/viewer?owner=chriswmackey&fork=hydra_2&id=Trees_in_Outdoor_Thermal_Comfort&slide=0&scale=6.062866266041592&offset=-2887.559959576377-582.9333700083878.
Chris Mackey. (2016b). Outdoor Microclimate Map (Code Example) [Computer Software]. http://hydrashare.github.io/hydra/viewer?owner=chriswmackey&fork=hydra_2&id=Outdoor_Microclimate_Map&slide=0&scale=1&offset=0.0.
Mackey, C., Roudsari, M.S., 2023. Ladybug Tools (1.6) [Python; Windows]. https://www.ladybug.tools/index.html#header-slide-show.
Mackey, C., Roudsari, M.S., Samaras, P., 2015. ComfortCover: a novel method for the design of outdoor shades. Simul. Ser. 47, 111–118.
Mardaljevic, J., 2011, August 23. Ambient calculation: *:* crash course [semiinar]. In: 10th International Radiance Workshop. Universoty of California, Berkeley Lab, United States of America. https://www.radiance-online.org/community/workshops/2011-berkeley-ca/presentations/day1/JM_AmbientCalculation.pdf.
Matzarakis, A., Rutz, F., Mayer, H., 2010. Modelling radiation fluxes in simple and complex environments: basics of the RayMan model. Int. J. Biometeorol. 54 (2), 131–139. https://doi.org/10.1007/s00484-009-0261-0.
McNeel, R., Others, 2010. Rhinoceros *3D* (Version 7) [Python]. Robert McNeel & Associates. https://www.rhino3d.com/.
McRae, I., Freedman, F., Rivera, A., Li, X., Dou, J., Cruz, I., Ren, C., Dronova, I., Fraker, H., Bornstein, R., 2020. Integration of the WUDAPT, WRF, and ENVI-met models to simulate extreme daytime temperature mitigation strategies in San Jose, California. Build. Environ. 184, 107180 https://doi.org/10.1016/j.buildenv.2020.107180.

Meggers, F., Kim, A., Rucewicz, S., Merchant, C., Chen, K., Teitelbaum, E., 2022. Improving mean radiant temperatures sensing using multidirectional non-contacting temperature sensors to avoid convective errors with globe thermometers. In: 2022 IEEE International Workshop on Metrology for Living Environment (MetroLivEn), pp. 18–22. https://doi.org/10.1109/MetroLivEnv54405.2022.9826986.

Meili, N., Manoli, G., Burlando, P., Carmeliet, J., Chow, W.T.L., Coutts, A.M., Roth, M., Velasco, E., Vivoni, E.R., Fatichi, S., 2021. Tree effects on urban microclimate: diurnal, seasonal, and climatic temperature differences explained by separating radiation, evapotranspiration, and roughness effects. Urban For. Urban Green. 58, 126970 https://doi.org/10.1016/j.ufug.2020.126970.

Merchant, C., Meggers, F., Hou, M., Aviv, D., Schneider, F.A., Middel, A., 2022. Resolving radiant: combining spatially resolved longwave and shortwave measurements to improve the understanding of radiant heat flux reflections and heterogeneity. Front. Sustain. Cities 4, 869743. https://doi.org/10.3389/frsc.2022.869743.

Middel, A., Selover, N., Hagen, B., Chhetri, N., 2016. Impact of shade on outdoor thermal comfort—A seasonal field study in Tempe, Arizona. Int. J. Biometeorol. 60 (12), 1849–1861. https://doi.org/10.1007/s00484-016-1172-5.

Middel, A., AlKhaled, S., Schneider, F.A., Hagen, B., Coseo, P., 2021. 50 grades of shade. Bull. Am. Meteorol. Soc. 102 (9), E1805–E1820. https://doi.org/10.1175/BAMS-D-20-0193.1.

Nicholson, S., Nikolopoulou, M., Watkins, R., 2023. Data-driven design for climate adaptation: validating ladybug tools for street-scale microclimate design. Will Cities Survive?, 2, 6.

Nikolopoulou, M., Lykoudis, S., 2006. Thermal comfort in outdoor urban spaces: analysis across different European countries. Build. Environ. 41 (11), 1455–1470. https://doi.org/10.1016/j.buildenv.2005.05.031.

O'Callaghan, P.W., Probert, S.D., 1977. Sol-air temperature. Appl. Energy 3 (4), 307–311. https://doi.org/10.1016/0306-2619(77)90017-4.

OpenCFD Ltd, 2022. *OpenFOAM* (Version 2212) [C++; Windows]. OpenFOAM Foundation. https://www.openfoam.com/.

Palomo Amores, T.R., Sánchez Ramos, J., Guerrero Delgado, M., Castro Medina, D., Cerezo-Narvaéz, A., Álvarez Domínguez, S., 2023. Effect of green infrastructures supported by adaptative solar shading systems on livability in open spaces. Urban For. Urban Green. 82, 127886 https://doi.org/10.1016/j.ufug.2023.127886.

Pham, J.V., Baniassadi, A., Brown, K.E., Heusinger, J., Sailor, D.J., 2019. Comparing photovoltaic and reflective shade surfaces in the urban environment: effects on surface sensible heat flux and pedestrian thermal comfort. Urban Clim. 29, 100500 https://doi.org/10.1016/j.uclim.2019.100500.

Robinson, D., Haldi, F., Kämpf, J., Leroux, P., Perez, D., Rasheed, A., Wilke, U., 2009. CITYSIM: Comprehensive Micro-Simulation of Resources Flows for Sustainable Urban Planning, pp. 1083–1090.

Rodonò, G., Naboni, E., Sapienza, V., Cucchi, F., Macrelli, G., 2020. Simulation workflow for parametric optimization of outdoor comfort-based origami shelter. J. Archit. Eng. 26 (3), 04020022 https://doi.org/10.1061/(ASCE)AE.1943-5568.0000410.

Rossi, F., Cardinali, M., Gambelli, A.M., Filipponi, M., Castellani, B., Nicolini, A., 2020. Outdoor thermal comfort improvements due to innovative solar awning solutions: an experimental campaign. Energ. Build. 225, 110341 https://doi.org/10.1016/j.enbuild.2020.110341.

Rossi, F., Cardinali, M., Di Giuseppe, A., Castellani, B., Nicolini, A., 2022. Outdoor thermal comfort improvement with advanced solar awnings: subjective and objective survey. Build. Environ. 215, 108967 https://doi.org/10.1016/j.buildenv.2022.108967.

San Maurizio Canavese, 2023. Italy Weather History | Weather Underground. https://www.wunderground.com/history/monthly/it/san-maurizio-canavese/LIMF/date/2023-7.

Santamouris, M., 2021. Present and future challenges and opportunities in the built environment. In: Chiesa, G. (Ed.), Bioclimatic Approaches in Urban and Building Design. Springer International Publishing, pp. 111–116. https://doi.org/10.1007/978-3-030-59328-5_5.

Santos Nouri, A., Costa, J., Santamouris, M., Matzarakis, A., 2018. Approaches to outdoor thermal comfort thresholds through public space design. A review. Atmosphere 9 (3), 3. https://doi.org/10.3390/atmos9030108.

Sedghy, F., Varasteh, A.-R., Sankian, M., Moghadam, M., 2018. Interaction between air pollutants and pollen grains: the role on the rising trend in allergy. Rep. Biochem. Mol. Biol. 6 (2), 219–224.

Shashua-Bar, L., Pearlmutter, D., Erell, E., 2011. The influence of trees and grass on outdoor thermal comfort in a hot-arid environment: influence of trees and grass on outdoor thermal comforT. Int. J. Climatol. 31 (10), 1498–1506. https://doi.org/10.1002/joc.2177.

Sun, R., Liu, J., Lai, D., Liu, W., 2023. Building form and outdoor thermal comfort: inverse design the microclimate of outdoor space for a kindergarten. Energ. Build. 284, 112824 https://doi.org/10.1016/j.enbuild.2023.112824.

Tang, P., Li, Q., 2022. Evaluation of the observation methods of outdoor mean radiant temperature in a subtropical city. Build. Environ. 207, 108462 https://doi.org/10.1016/j.buildenv.2021.108462.

The Weather Company, 2023. PWS Network Overview. Weather Underground. https://www.wunderground.com/history/monthly/it/san-maurizio-canavese/LIMF/date/2023-7.

Thorsson, S., Lindqvist, M., Lindqvist, S., 2004. Thermal bioclimatic conditions and patterns of behaviour in an urban park in Goteborg, Sweden. Int. J. Biometeorol. 48 (3), 149–156. https://doi.org/10.1007/s00484-003-0189-8.

Toparlar, Y., Blocken, B., Maiheu, B., Van Heijst, G.J.F., 2017. A review on the CFD analysis of urban microclimate. Renew. Sust. Energ. Rev. 80, 1613–1640. https://doi.org/10.1016/j.rser.2017.05.248.

U.S. Department of Energy. (2022a). Energy Plus Version 22.1.0 Documentation: Engineering Reference. University of Illinois and Lawrence Berkeley National Laboratory. chrome-extension://efaidnbmnnnibpcajpcglclefindmkaj/https://energyplus.net/assets/nrel_custom/pdfs/pdfs_v22.1.0/EngineeringReference.pdf.

U.S. Department of Energy, 2022b. EnergyPlus (22.2.0) [Computer Software]. U.S. Department of Energy Building Technologies Office. https://energyplus.net/.

Van Ameijde, J., Ma, C.Y., Goepel, G., Kirsten, C., Wong, J., 2022. Data-driven placemaking: public space canopy design through multi-objective optimisation considering shading, structural and social performance. Front. Architect. Res. 11 (2), 308–323. https://doi.org/10.1016/j.foar.2021.10.007.

Vartholomaios, A., Kalogirou, N., 2020. Optimisation of outdoor shading devices with thermal comfort criteria: the case of the venetian port of Chania. IOP Conf. Ser. Earth Environ. Sci. 410 (1), 012058 https://doi.org/10.1088/1755-1315/410/1/012058.

Watanabe, S., Nagano, K., Ishii, J., Horikoshi, T., 2014. Evaluation of outdoor thermal comfort in sunlight, building shade, and pergola shade during summer in a humid subtropical region. Build. Environ. 82, 556–565. https://doi.org/10.1016/j.buildenv.2014.10.002.

Weeding, B., Love, P., Beyer, K., Lucieer, A., Remenyi, T., 2024. High-resolution projections of outdoor thermal stress in the twenty-first century: a Tasmanian case study. Int. J. Biometeorol. https://doi.org/10.1007/s00484-024-02622-8.

Weytjens, L., Attia, S., Verbeeck, G., De Herde, A., 2011. The 'Architect-friendliness' Of Six Building Performance Simulation Tools: A Comparative Study. International Journal of Sustainable Building Technology and Urban Development 2 (3), 237–244. https://doi.org/10.5390/SUSB.2011.2.3.237.

Yuan, J., Masuko, S., Shimazaki, Y., Yamanaka, T., Kobayashi, T., 2022. Evaluation of outdoor thermal comfort under different building external-wall-surface with different reflective directional properties using CFD analysis and model experiment. Build. Environ. 207, 108478 https://doi.org/10.1016/j.buildenv.2021.108478.

Zhang, J., Gou, Z., Zhang, F., Yu, R., 2023. The tree cooling pond effect and its influential factors: a pilot study in Gold Coast, Australia. Nat. Based Solut. 3, 100058 https://doi.org/10.1016/j.nbsj.2023.100058.